Research Paper

THEMED ISSUE: Anatomy of Rifting: Tectonics and Magmatism in Continental Rifts, Oceanic Spreading Centers, and Transforms

GEOSPHERE

GEOSPHERE; v. 14, no. 4

https://doi.org/10.1130/GES01615.1

12 figures; 1 set of supplemental files

CORRESPONDENCE: chiasera@msu.edu

CITATION: Chiasera, B., Rooney, T.O., Girard, G., Yirgu, G., Grosfils, E., Ayalew, D., Mohr, P., Zimbelman, J., and Ramsey, M.S., 2018, Magmatically assisted off-rift extension—The case for broadly distributed strain accommodation: Geosphere, v. 14, no. 4, p. 1544–1563, https://doi.org/10.1130/GES01615.1.

Science Editor: Shanaka de Silva
Guest Associate Editor: Carolina Pagli

Received 15 September 2017
Revision received 28 February 2018
Accepted 15 May 2018
Published online 11 July 2018

Magmatically assisted off-rift extension—The case for broadly distributed strain accommodation

Brandon Chiasera[1], Tyrone O. Rooney[1], Guillaume Girard[1], Gezahegn Yirgu[2], Eric Grosfils[3], Dereje Ayalew[2], Paul Mohr[4], James R. Zimbelman[5], and Michael S. Ramsey[6]

[1]Department of Earth and Environmental Sciences, Michigan State University, East Lansing, Michigan 48824, USA
[2]Department of Earth Sciences, Addis Ababa University, Addis Ababa, Ethiopia
[3]Geology Department, Pomona College, Claremont, California 91711, USA
[4]Tonagharraun, Corrandulla, County Galway, Ireland
[5]CEPS/NASM MRC 315, Smithsonian Institution, Washington D.C., 20013–7012, USA
[6]Department of Geology and Planetary Science, University of Pittsburgh, Pittsburgh, Pennsylvania 15260-3332, USA

ABSTRACT

Within continental rift settings, extensional strain is initially accommodated along the nascent rift margins, subsequently localizing to zones of focused magmatic intrusion. The migration of strain from rift-border faults to diking places an emphasis on constraining the magmatic plumbing system of zones of focused intrusion to resolve how extension is accommodated in the rift lithosphere. While existing rifting models concentrate on the relationship between extension and focused magmatism within the rift, there is increasing evidence of rift-related magmatic activity outside the rift valley. We examine the Galema range, an area of focused magmatic activity along the eastern margin of the Central Main Ethiopian Rift, which is morphologically similar to areas of focused magmatism within the rift. We find that whole-rock thermodynamic modeling and thermobarometric calculations on mineral-liquid pairs suggest that fractionation (and hence magma stalling depths) within the Galema range is polybaric (~7 and ~3 kbar). These results, when compared to zones of focused intrusion within the rift, indicate an incipient magmatic plumbing system. We contend that diking associated with the Galema range, which predates magmatic belts within the rift, thermomechanically modified the lithosphere along this margin. While the cessation of magmatism within the Galema range may have been precipitated by a change in magma flux, the now thermomechanically modified lithospheric mantle along this margin facilitated the subsequent development of within-rift magmatic chains. The implications of this are that off-rift magmatic activity may play an integral role in facilitating the development of rift architecture.

1. INTRODUCTION

As a continental rift progresses toward an oceanic spreading center, the mechanism of strain accommodation must transition from faulting and thinning of the lithosphere to focused magmatic intrusion (Buck, 2004; Buck, 2006; Casey et al., 2006; Corti, 2009, 2012; Mazzarini et al., 2013; Rooney, 2010; Rooney et al., 2014; Wolfenden et al., 2005). Specifically, strain is thought to migrate from high-angle border faults to zones of focused magmatic activity within the rift that are adjacent to the rift-border faults (Ebinger and Casey, 2001). Though the specific mechanisms remain controversial, these zones of focused magmatic intrusion must eventually migrate toward the rift axis as possible precursors to oceanic spreading centers (Ebinger, 2005). While elegant in its simplicity, observations from rifting environments reveal magmatic features that are unexplained by this model. For example, magmatism outside of the rift proper is frequently observed to be contemporaneous with episodes of both mechanical extension and focused magmatic intrusion within the rift (Abebe et al., 1998; Keranen and Klemperer, 2008). Seemingly related to the rifting process, this magmatism is not adequately explained by the currently accepted models of continental rifting.

The East African Rift System (EARS) preserves within it a broad range of rifting morphologies from incipient rifting in the south to the transition from continental to oceanic crust in the north (Corti, 2009; Ebinger, 2005; Ebinger and Casey, 2001; Gregory et al., 1896; Gregory, 1920; Sueß, 1891; Woldegabriel et al., 1990). The existing models of strain accommodation within continental rifting settings were borne of studies of the EARS. As studies of this system progressed, the initial models of rift-centered strain accommodation have evolved into models where the extensional strain is accommodated both by the rift-border faults and the magmatic belts within them (Ebinger, 2005; Wolfenden et al., 2005). The amount of extensional strain that is accommodated by the rift-border faults and magmatic belts, and the timing of this accommodation, remain controversial (e.g., Agostini et al., 2011a; Bendick et al., 2006; Bilham et al., 1999; Casey et al., 2006; Molin and Corti, 2015; Pizzi et al., 2006). The Main Ethiopian Rift (MER), located directly south of Afar, is a transitional region whereby strain is accommodated both by rift-border faults and focused magmatic intrusion (Casey et al., 2006; Corti, 2009; Ebinger and Casey, 2001; Pizzi et al., 2006) (Fig. 1A). Within the Main Ethiopian Rift, recent magmatic activity has been focused along linear belts known as the Silti-Debre Zeyit Fault Zone (SDFZ) and the Wonji Fault Belt (WFB) (Acocella et al., 2003; Bonini et al., 2005; Casey et al., 2006; Corti, 2009; Ebinger and Casey, 2001; Kurz et al., 2007; Mohr, 1962; Morton et al., 1979; Rooney et al., 2007; Rooney

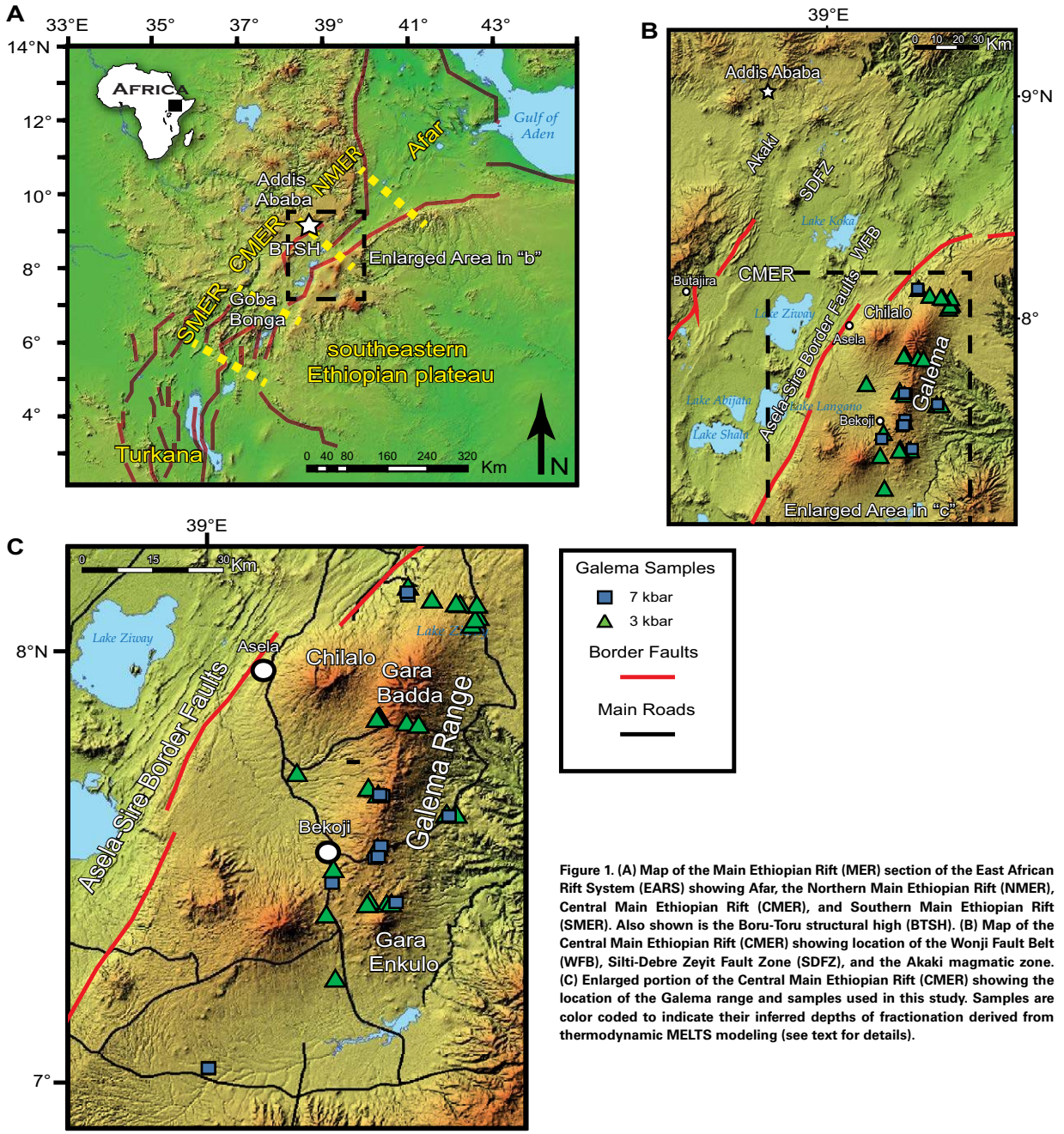

Figure 1. (A) Map of the Main Ethiopian Rift (MER) section of the East African Rift System (EARS) showing Afar, the Northern Main Ethiopian Rift (NMER), Central Main Ethiopian Rift (CMER), and Southern Main Ethiopian Rift (SMER). Also shown is the Boru-Toru structural high (BTSH). (B) Map of the Central Main Ethiopian Rift (CMER) showing location of the Wonji Fault Belt (WFB), Silti-Debre Zeyit Fault Zone (SDFZ), and the Akaki magmatic zone. (C) Enlarged portion of the Central Main Ethiopian Rift (CMER) showing the location of the Galema range and samples used in this study. Samples are color coded to indicate their inferred depths of fractionation derived from thermodynamic MELTS modeling (see text for details).

et al., 2014; Rooney et al., 2005; Woldegabriel et al., 1990; Wolfenden et al., 2004) (Fig. 1B). While much attention has been given to the magmatic activity along these linear belts within the rift proper (Medynski et al., 2015; Rooney et al., 2007; Rooney, 2010; Rooney et al., 2011; Rooney et al., 2014), there is a growing realization that magmatic activity associated with rifting is more diffuse (e.g., Abebe et al., 1998; Meshesha and Shinjo, 2007; Rooney et al., 2016; Trestrail et al., 2016).

Here we undertake a petrographic and geochemical analysis of an area of focused magmatic intrusion on the Southeastern Ethiopian Plateau, which is interpreted to be contemporaneous with rift development but occurs outside of the Ethiopian Rift valley (Kennan et al., 1990; Mohr and Potter, 1976). The Galema range is a NNE-trending series of en echelon dikes, lavas, and eroded cinder cones, located ~35 km east of the Asela-Sire Border Fault (Fig. 1C). We focus upon constraining the magmatic plumbing system of the Galema range through the use of geochemical and petrographic analyses, offering insight into the architecture of the magmatic plumbing system in which the magma ascended and the depths of crystal phase fractionation. The depths at which a magma commonly stalls on ascent are, in part, determined by the extensional stresses acting on the lithosphere at the time, and these volumes at depth represent presumed zones of magmatic strain accommodation (Corti et al., 2003). In this manner, a profile of the lithospheric strain at an off-rift location may be constructed. Our results demonstrate that the Galema range accommodated extensional strain after the initial formation of the border faults that define the rift, but before the inception of zones of focused magmatic intrusion within the rift (i.e., WFB and SDFZ). This suggests that strain accommodation by focused magmatic intrusion can occur over a broad area in continental extension settings. Furthermore, the emplacement of the Galema range also shows that migration of focused magmatic activity toward the rift axis is not always a straightforward progression as some models of continental rifting evolution assert.

2. BACKGROUND

2.1. Cenozoic Magmatic Evolution of the African-Arabian Large Igneous Province

Cenozoic magmatic activity in East Africa commenced in the Eocene with basaltic volcanism in the broadly rifted zone in the Turkana area of northern Kenya and southern Ethiopia at ca. 45 Ma (Corti, 2009; Ebinger et al., 1993; George and Rogers, 2002) (Fig. 1A). Large-scale flood basalts were emplaced during the Oligocene as a result of the impingement of the Afar plume (Baker et al., 1996; Hofmann et al., 1997; Kieffer, 2004; Pik et al., 1999; Rochette et al., 1998). In the early Miocene, a resurgence of volcanism occurred throughout the region, with increased basaltic activity in Turkana and both shield volcanism and fissure-fed basalts on the Ethiopian Plateau (Rooney, 2017). Subsequent magmatism was largely localized to the developing MER and took the form of large silicic centers and smaller basaltic eruptions (Rooney et al., 2011).

2.2. Development of the Main Ethiopian Rift (MER)

The MER runs from Afar in northeastern Ethiopia to Turkana in Kenya and changes from a ~NE-SW trend in the north to a ~N-S trend in the south. The MER is divided into three sectors: the Northern Main Ethiopian Rift (NMER), the Central Main Ethiopian Rift (CMER), and the Southern Main Ethiopian Rift (SMER) (Corti, 2009; Woldegabriel et al., 1990) (Fig. 1A). These sectors evolved at different times and into a nonlinear trend (Abebe et al., 2010; Balestrieri et al., 2016; Bonini et al., 2005; Corti, 2009; Keranen and Klemperer, 2008; Woldegabriel et al., 1990; Wolfenden et al., 2004).

The CMER is bounded by the Boru-Toru structural high and the Goba-Bonga structural lineament (Bonini et al., 2005) (Fig.1A). The main border fault in this area of the CMER, known as the Asela-Sire Border Fault, is a segmented system of high-angle, normal faults (>60°) that define the MER. These faults trend at approximately N30°E–N40°E, separating the CMER from the Southeastern Ethiopian Plateau (Abebe et al., 2010; Boccaletti et al., 1998; Woldegabriel et al., 1990) and are mid-Miocene (Ebinger and Casey, 2001), no older than ca. 8 Ma (Abebe et al., 2010; Bonini et al., 2005; Woldegabriel et al., 1990).

2.3. Methods of Extensional Strain Accommodation in the CMER

The Asela-Sire Border Faults formed during the southward propagation of rifting from Afar (Abebe et al., 2007; Bonini et al., 2005; Keranen and Klemperer, 2008). The N-S trend of the Asela-Sire Border Faults led to the interpretation that the orientation of extensional stress had rotated to roughly E-W from the previous NW-SE direction (Boccaletti et al., 1998; Bonini et al., 2005). It should be noted that this difference in trend has been attributed, not to rotation of the stress field, but to the interference of preexisting lithospheric weaknesses interacting with an extensional stress field oblique to the trend of the rift (Agostini et al., 2011b; Corti, 2008; Corti et al., 2013). Postdating the initiation of the Asela-Sire Border Faults, the magmatic activity within the CMER was focused on the Quaternary Wonji Fault Belt (WFB) and the Silti-Debre Zeyit Fault Zone (SDFZ) (Mohr, 1962; Rooney et al., 2014; Woldegabriel et al., 1990) (Fig. 1B). While the WFB accommodates some of the extensional strain in the CMER, the Asela Sire rift-border faults also currently continue to accommodate a portion of this strain (Agostini et al., 2011a; Corti, 2009; Pizzi et al., 2006). However, the amount of extensional strain accommodated by the rift-border faults and the timing of this strain accommodation by both mechanisms remain controversial.

Analysis of the river network patterns in the CMER indicates that a portion of the extensional strain is accommodated by the Asela-Sire Border Faults (Molin and Corti, 2015). GPS velocities show that the recent extension rate across the MER is ~4.0 ± 0.9 mm/yr, accommodated by both mechanical stretching and faulting of the lithosphere as well as aseismic dike injection (Bendick et al., 2006).

Structural analysis of the CMER indicates that the Aslea-Sire border faults have recently accommodated extensional strain—as recorded by fault-slip data recorded across the rift (Agostini et al., 2011a). This analysis also indicates that extensional strain accommodation of the WFB, via faulting of the crust, is subordinate to that accommodated at the eastern rift-border fault. However, forces exerted by the magma overpressure of an intruding dike can reduce the amount of observable slip along nearby faults (Rubin and Pollard, 1988). The compressive force exerted by the intruding dike in the direction of σ_3, as a result of the buoyancy of an ascending magma, can change the local stress field in the host rock by increasing compression to each side of the dike and reducing compression above (Rubin and Pollard, 1988). One consequence of this is that preexisting faults that are located adjacent to the intruding dike (i.e., those not generated by intrusion of the dike) can become locked (Rubin and Pollard, 1988). Exploitation of preexisting faults by magmatic intrusion on ascent adds volume to the host rock, accommodating extensional strain (Rubin and Pollard, 1988). In areas experiencing both faulting and intrusion (such as the WFB), the total amount of deformation is partitioned between fault-slip and volumetric increase, but the observable amount of fault-slip appears to be reduced, complicating estimates of the amount of strain accommodation by faulting.

2.4. Magmatic Strain Accommodation during the Plio-Quaternary

2.4.1. Wonji Fault Belt and Silti-Debre Zeyit Fault Zone

The Wonji Fault Belt (WFB), located near the eastern rift margin and subparallel to the rift axis in the CMER, is described as a series of right-stepping, en echelon faults and dikes within the rift, which are interpreted to be <1.8 Ma (Ebinger and Casey, 2001; Woldegabriel et al., 1990; Wolfenden et al., 2004). The volcanism of the WFB is described as being bimodal in nature with silicic volcanism, sometimes forming large calderas, and basaltic volcanism forming lava flows and scoria cones (Kurz et al., 2007; Mohr, 1967; Mohr et al., 1980; Rooney et al., 2005).

Located toward the western rift margin, the SDFZ is characterized as a linear chain of nested calderas, scoria cones, and basaltic flows with associated silicic centers also oriented subparallel to the rift axis (Gasparon et al., 1993; Rooney et al., 2007; Rooney et al., 2011; Rooney et al., 2005; Woldegabriel et al., 1990).

The locations of both the WFB and SDFZ along the rift margins may be due to the existence of preexisting lithospheric weaknesses within the MER. When a low-obliquity extensional stress field is applied to these weaknesses, the result is formation of boundary faults oblique to the extension direction, followed by formation of internal faults nearly perpendicular to the direction of extension (Agostini et al., 2009; Agostini et al., 2011b; Corti, 2008). Analog modeling of stress direction oblique to preexisting lithospheric weakness suggests that the WFB in the CMER represents an intermediate stage of rift development (Agostini et al., 2011b).

2.4.2. The Galema Range

We focus on the Galema range, an area of Pliocene, rift-adjacent magmatism on the Southeastern Ethiopian Plateau (Fig. 1C). Located ~130 km southeast of Addis Ababa, it occurs to the east of the border faults that define the rift valley in the CMER (Fig. 1C). Morphologically, the Galema range displays striking similarities to magmatic features located within the rift valley of the MER. For example, the Galema range consists of a series of right stepping, en echelon mafic dikes trending at ~10°–20°N and aligned, eroded scoria cones (Mohr, 1980; Mohr and Potter, 1976; Woldegabriel et al., 1990), similar to the WFB. The Galema range extends from the volcanic center in the north known as Gara Badda to the volcanic center in the south known as Gara Enkulo (Fig. 1C). The dikes, which constitute the range, span a distance of ~70 km and are arranged in a dextral, en echelon formation within a ~7-km-wide fissure system (Mohr and Potter, 1976). Maars and cinder cones exist between the two volcanic centers, along with the ~4.5-m-thick dikes that gradually disappear at the latitude of Gara Enkulo (Mohr and Potter, 1976). The Galema range rises to an elevation ~1000 m above the Southeastern Ethiopian Plateau and is comprised of the magmatic pile erupted from the dikes and silicic centers (Mohr and Potter, 1976). Evidence of this volcanism can be found in the volcanic edifices that appear within the Galema range. Volcanic edifices within the WFB are dominantly of two varieties: cinder cones and large silicic centers. The Galema range preserves within it volcanic necks of silicic composition, which are the exposed magmatic plumbing system of large silicic centers (Fig. 2). Moreover, the scoria cones found within the WFB are rooted by dikes; the exposed dikes evident in the Galema range are parallel to the magmatic plumbing system of these scoria cones. Field work has revealed eroded scoria cones in the southern portion of the study area (Mohr and Potter, 1976).

While the magmatic features of the Galema range and the WFB display striking morphological similarities, the direct evidence of the existence of faulting of the Galema range is less apparent than that of the WFB. This may indicate that while both areas have accommodated extensional strain, the amount of strain accommodated by faulting in the Galema range may be less profound. Indirect evidence, however, suggests that faults existed prior to the onset of magmatic intrusion. Recent work has highlighted the influence of preexisting faults and fractures within the lithosphere on the morphology of dike swarms and volcanic fields (Le Corvec et al., 2013; Mazzarini et al., 2016). These studies indicate that in areas of relatively thicker crust, alignments of dikes and monogenetic vents (i.e., scoria cones) are parallel to the trend of preexisting lithospheric fractures and faults (Mazzarini et al., 2016). Thus, the alignment of dikes and scoria cones of the Galema range, in the area of thicker crust (see section 5.5) of the Eastern Ethiopian Plateau, suggest that the ascending mafic dikes exploited preexisting lithospheric faults and fractures. As the ascending dikes are captured by the preexisting faults (Le Corvec et al., 2013), evidence of the existence of these faults may be obscured as they are cut by the intruding magma (Rubin and Pollard, 1988).

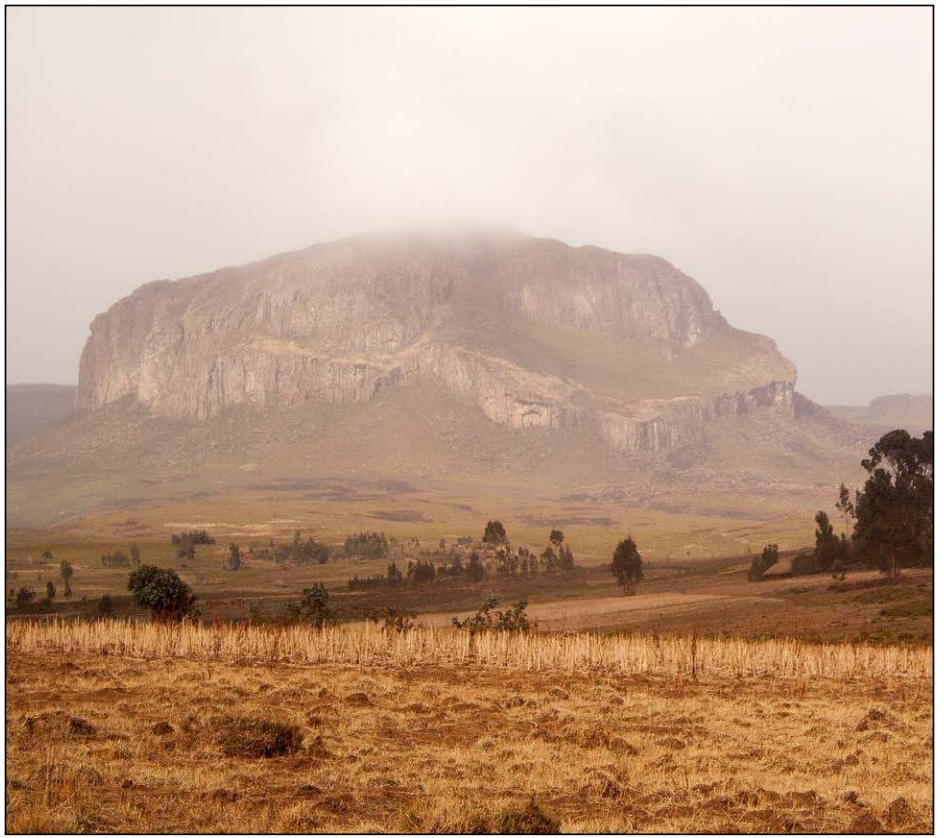

Figure 2. Photograph of a silicic center in the Galema range displaying evidence of the volcanic activity that built up the relief of the range before erosion. Photograph courtesy of T.O. Rooney. Taken at ~7.830685°N, 39.353445°E, looking east.

Glaciation during the middle to Late Pleistocene eroded the up to 2000-m-thick magma pile and exposed the dikes that had fed the cinder cones of the Galema range (Mohr and Potter, 1976). Taken together, it is evident that the magmatic plumbing systems of both silicic and mafic edifices are exposed within the Galema range. It is important to note that such erosion would have removed all evidence of faulting induced above propagating dikes, as mentioned earlier. The implication of such erosion would be the preservation of a magmatic plumbing system, broadly similar to that beneath the modern WFB, but devoid of clear evidence of faulting.

K-Ar dating of samples of the Galema range yielded dates of formation at ca. 2.1 to ca. 3.1 Ma (Mohr and Potter, 1976) and 1.97 ± 0.02 Ma (Kennan et al., 1990). The existence of off-rift zones of focused intrusion such as the Galema range is not well constrained within the current rifting framework but has been attributed to the possible existence of preexisting lithospheric structures (Corti, 2012; Mohr and Potter, 1976).

3. METHODS

3.1. Whole-Rock Geochemical Analysis

A field excursion in 2008 recovered 77 samples from dikes, basaltic flows, scoria cones, and silicic centers of the Galema range. These samples were cut to minimize alteration due to weathering before being further cut into ~30 g billets. After polishing to remove saw marks and cleaning in an ultrasonic bath of deionized water, the billets were crushed in a steel jaw crusher and then powdered in a Bico ceramic disk mill. The powders were then fused with a lithium tetraborate ($Li_2B_4O_7$) flux into glass discs, following procedures detailed elsewhere (e.g., Rooney et al., 2012). Major-element oxide abundances and loss-on-ignition values were determined via X-ray fluorescence analysis on a Bruker S4 Pioneer instrument at Michigan State University (Supplemental Tables[1]).

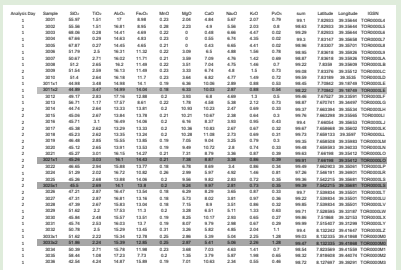

[1]Supplemental Tables. Tables of XRF and LA-ICP-MS results used in this study, including example calculations for mineral chemistry averaging and analysis of reproducibility of in-situ spot ablation. Please visit https://doi.org/10.1130/GES01615.S1 or the full-text article on www.gsapubs.org to view the Supplemental Tables.

3.2. In Situ LA-ICP-MS Mineral Analysis

Analyses of clinopyroxene and plagioclase mineral phases were performed on a representative subset of samples ranging from primitive to evolved compositions, on the basis of their bulk-rock MgO content, using in situ spot analyses by laser ablation–inductively coupled plasma–mass spectrometry (LA-ICP-MS) following protocols developed together with other studies (Rooney et al., 2016; Trestrail et al., 2016). Standard petrographic thin sections were loaded into a 15 × 15 cm two-volume HelEx sample cell, integral to a Teledyne Photon Machines Analyte G2 193 nm excimer laser ablation system at Michigan State University. Multiple spots of 110 µm diameter in individual crystals were ablated for 30 s with a laser repetition rate of 10 Hz at a fluence of 4.1 J/cm^2. A gas blank was collected after each sample for ~20 s, and gas blank intensities were subtracted from ablation intensities. The ablated material was transferred to a Thermo Scientific ICAP Q quadrupole ICP-MS in a flux of 0.75 L/min of high-purity He carrier gas for analysis. The ICP-MS was tuned for highest intensities, low-oxide production rate (ThO/Th < 0.7%), and low double-charged cation formation rate (Ba^{2+}/Ba <1.5%) by performing surface scans of National Institute of Standards and Technology (NIST) SRM 612 glass standard, while signal stability was subsequently tested over a 3 min surface scan of NIST SRM 612. Data were calibrated using 20 natural and synthetic geological standards (Supplemental Tables [footnote 1]) mounted on the same sample tray together with the samples. These were analyzed sequentially without opening the sample chamber and interrupting automation. Data were collected using the ICP-MS in kinetic energy discrimination mode in which the ionized material circulates through a collision cell fluxed with He, reducing isobaric interferences with oxide and argide compounds, enhancing detection limits of light mass isotopes including major elements, and lowering their signal intensities, allowing for their quantification at a precision and accuracy similar to trace elements (Supplemental Tables). Data were drift corrected using surface scans of well-characterized fused rock powder standards (JB-1a and BHVO-1) analyzed approximately every hour during analysis at 10 µm/s and other ablation parameters identical to those described above. Replicated analyses of JB-1a and BHVO-1 analyzed as unknowns by surface-scan analyses achieved ±5% accuracy and day-averaged reproducibility of 5% (1σ) or better (Supplemental Tables). The raw sum of all major-element oxides with Fe expressed as FeO was calculated for each mineral analysis, in order to normalize all major- and trace-element compositions to 100 wt% oxides. Practically, 100 wt% oxides was our internal standard for all mineral analyses; such an assumption is reasonable for all stoichiometrically anhydrous minerals. If necessary, certain laser ablation signals were then filtered to remove certain sections of ablation sequences exhibiting evidence of micro-crystal inclusions and or alteration. Reproducibility of the in situ spot analyses was assessed separately by performing ten 30-second ablations on each of the basalt glass standards GSD-1G and BCR-2G for major and trace elements using analytical conditions identical to those above; on these homogeneous glass materials, reproducibility is also generally of 5% (1σ) or better (Supplemental Tables).

4. RESULTS

4.1. Petrography

In hand sample, the mafic specimens collected from the Galema range can be described as massive, non-vesicular basalts with sparse, 1–5 mm–scale plagioclase crystals. A subset of samples is scoriaceous with visible plagioclase crystals at the 1–5 mm scale. As a whole, the samples show little to no evidence of alteration or magma mingling at hand-sample scale.

In thin section, a majority of the samples collected from the Galema range exhibit crystal phases dominated by plagioclase, and a lesser abundance of samples display olivine as the primary crystal phase. A subset of samples includes clinopyroxene crystals as part of the phenocryst population (Fig. 3). These crystal phases rarely display resorption or skeletal textures, and most appear to be in equilibrium with the ground mass, while none display evidence of zoning (Fig. 4) (Supplemental Tables [footnote 1]). All samples are observed to contain plagioclase laths within a cryptocrystalline to aphanitic groundmass. Opaque Fe-Ti oxide crystals also occur as a fractionating phase in all samples in plane polarized light. Anhedral olivine crystals occur as part of the mineral assemblage in varying abundances in samples with >~2.5 wt% MgO, appearing as the primary mineral phase in samples with >~9.0 wt% MgO, though often altered to iddingsite (Figs. 3 and 4). Anhedral to subhedral clinopyroxene crystals occur as part of the phenocryst assemblage in samples with between ~7.0 wt% and ~8.0 wt% MgO (Figs. 3 and 4). Plagioclase crystals are present within the range of ~1.3 to ~9.6 MgO wt%. It is the primary mineral phase in samples from ~1.0 to ~4.5 MgO wt% and occurs in varying abundance with olivine between ~4.5–9.6 wt% MgO (Fig. 3).Within the Galema range, the temporal relationship between the silicic centers and mafic dikes is not well constrained, and we therefore focus on the mafic samples in an effort to characterize their magmatic plumbing systems. Samples with >~59 wt% SiO_2 (<~1.4 wt% MgO), as determined by X-ray fluorescence analysis, were not considered further.

4.2. Major-Element Geochemistry

On the basis of the total alkali silica diagram (Le Maitre et al., 2005), our samples from the Galema range plot in an array from picrobasalt to rhyolite (Fig. 5). The magmatic products of the Galema range have been described previously as bimodal in silica content, composed of hawaiites (trachybasalts) and comendites (rhyolites) (Mohr, 1980). There is a noticeable lack of samples with SiO_2 content between ~59 wt% to ~68 wt% (Supplemental Tables [footnote 1]) (Fig. 5). This lack of such sample compositions, also known as the Daly Gap, is described in many locations in the EARS (Baker, 1987; Peccerillo et al., 2003; Rooney et al., 2012; Trua et al., 1999). This gap has been interpreted as a function of differential tapping of magma chambers at depth (Peccerillo et al., 2007) and more recently as the result of a magma mush where more silicic material has evolved and removed from the magma chamber to fractionate and shallower levels (Rooney et al., 2012; Trua et al., 1999).

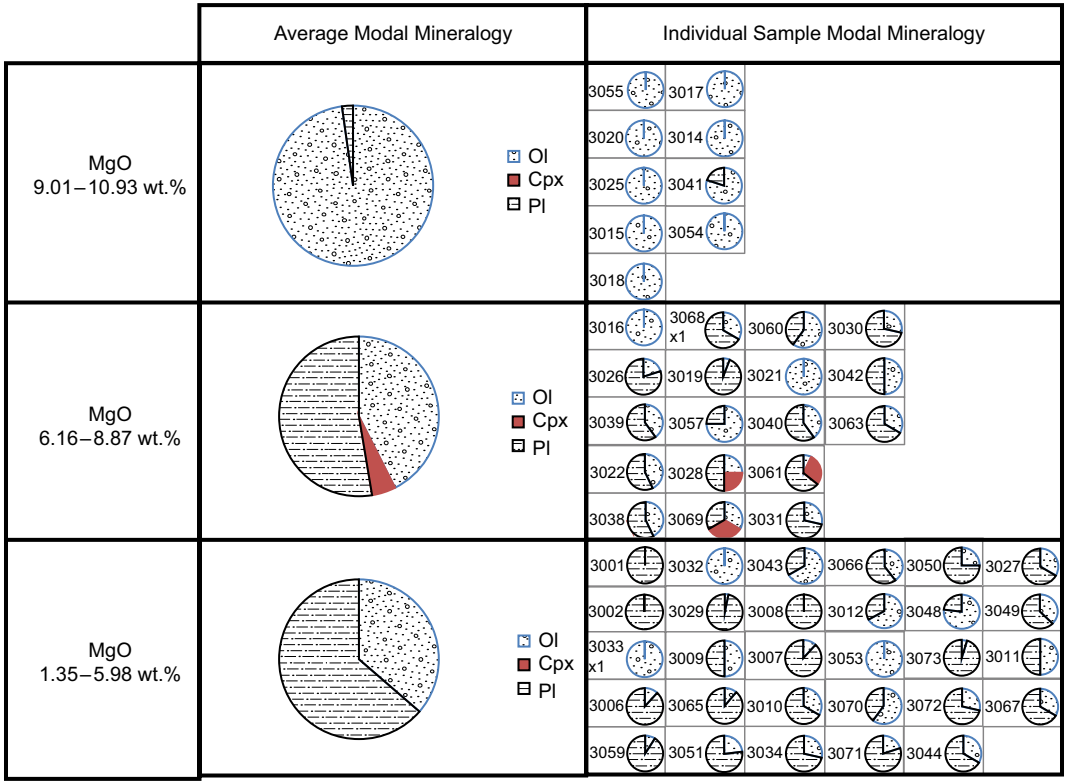

Figure 3. Chart showing the crystal phase distribution of samples from the Galema range. Divisions are based on the dominant crystal phase observed and reported in MgO wt%. Individual samples, which are components of the larger divisions, are also presented. Relative crystal phase abundances were normalized based on the observed phenocrysts. Groundmass or vesicle abundance not included.

Variation diagrams of the major-element geochemistry of samples with >~1.4 wt% MgO show trends consistent with fractional crystallization of olivine, plagioclase, pyroxene, and Fe-Ti oxides occurring over the course of magmatic evolution (Fig. 6). In samples with >~9 wt% MgO content, the relatively flat trend of Fe_2O_3 and TiO_2 versus MgO is consistent with crystallization of olivine. Crystallization of pyroxene occurs in the compositional range of ~6 to ~9 wt% MgO as indicated by the decreasing trend of CaO/Al_2O_3 versus MgO. Below ~5 wt% MgO, formation of Fe-Ti oxides is indicated by a break in slope of Fe_2O_3 and TiO_2 versus MgO (Fig. 6). Below ~6 wt% MgO, plagioclase is the primary fractionating phase as indicated by the slope of the CaO/Al_2O_3 versus MgO variation diagram.

4.3. Mineral Chemistry

Results of in situ LA-ICP-MS analysis on the crystal phases of samples selected for crystal availability from each of the pressure regimes determined in section 5.2.1 (3028, 3029, 3061, 3068, and 3072) reveal compositions confirming the observations in thin section of the presence of plagioclase and pyroxene phases (Supplemental Tables [footnote 1]). Multiple analyses of each crystal were performed, and data were averaged across each crystal because no significant core-to-rim zoning was observed (Supplemental Tables) (Fig. 4E). The size of the laser spot created an averaging effect of the crystal chemistry in each analysis, obscuring any chemical evidence of fine zoning for each crystal. After filtering the data that showed clear signs of inclusion and/or alteration, the crystal chemistry of each spot in an individual transect was analyzed for evidence of chemical zoning, and the standard deviation for each transect was calculated (Supplemental Tables) (Fig. 4E). These data were averaged to determine the average crystal chemistry. The averaging calculations allow for a more representative composition of the clinopyroxene phenocrysts in equilibrium with the melt, facilitating thermobarometric calculations.

Labradorite occurs as the most abundant plagioclase phase in samples 3029 (3.28 wt% MgO) ($An_{52–54}$), 3061 (7.94 wt% MgO) ($An_{63–65}$), and 3072 (4.86 wt% MgO) ($An_{51–56}$). Bytownite occurs as the most abundant plagioclase phase of sample 3068 (7.02 wt% MgO) ($An_{71–78}$) (Supplemental Tables [footnote 1]) (Fig. 7A).

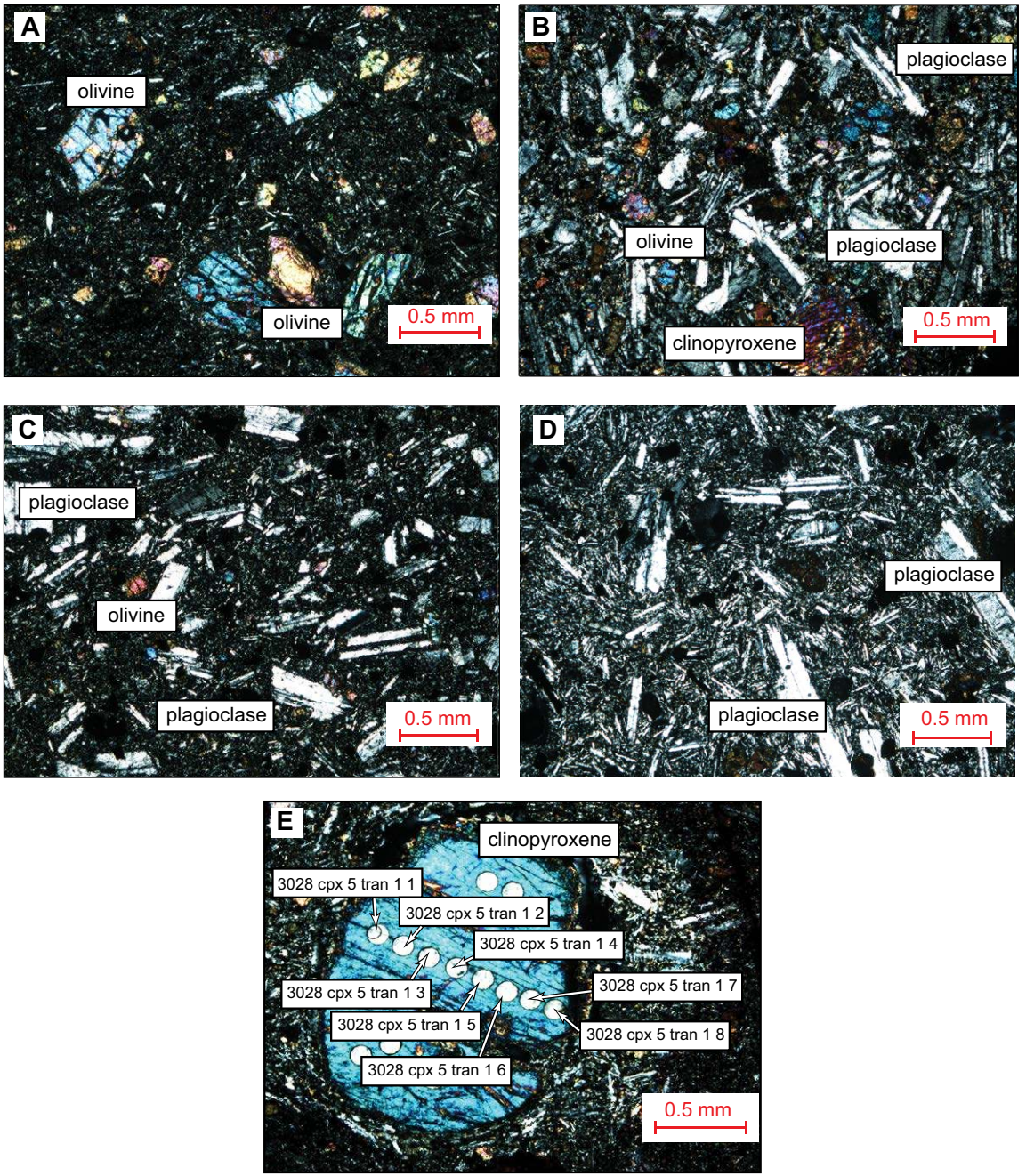

Figure 4. Photomicrographs showing the crystal phases of samples from the Galema range including olivine, clinopyroxene, and plagioclase phenocrysts. (A) Sample 3015 (10.21 wt% MgO); (B) sample 3061 (7.94 wt% MgO); (C) sample 3072 (4.86 wt% MgO); (D) sample 3029 (3.28 wt% MgO); and (E) clinopyroxene 5 from sample 3028 (7.15 wt% MgO). Circular impressions are locations where some of the laser ablation–inductively coupled plasma–mass spectrometry (LA-ICP-MS) analyses were performed. Labels indicate individual analyses of a transect, corresponding to data in Supplemental Tables (text footnote 1).

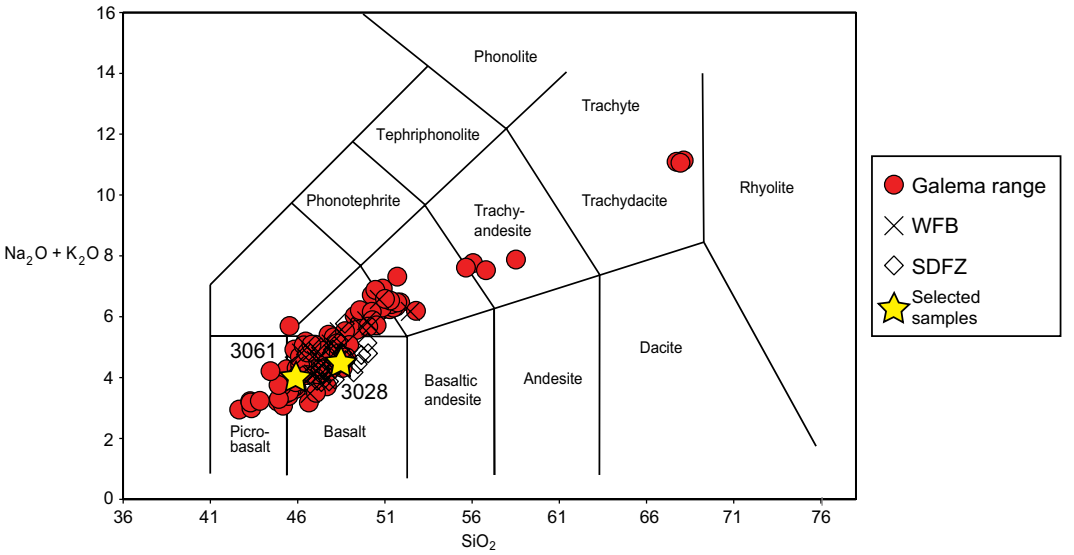

Figure 5. Total alkali silica (after Le Maitre et al., 2005) diagram showing the Galema range samples used in this study. Note the prominent lack of samples between ~59 and ~67 wt% SiO_2. See text for details. WFB—Wonji Fault Belt; SDFZ—Silti-Debre Zeyit Fault Zone.

The clinopyroxene phases of samples 3061 and 3028 (7.15 wt% MgO) are classified as augite with $Wo_{38–40}$, $Fs_{9–15}$ and $Wo_{38–42}$, $Fs_{11–16}$, respectively (Supplemental Tables) (Fig. 7B).

To determine whether the crystal phases are in equilibrium with the ground mass, and to choose suitable candidates for thermobarometric calculations, the in situ analyses were used in combination with the whole-rock X-ray fluorescence (XRF) analyses to calculate partition coefficient (K_D) values between crystal with melt. In sample 3061, K_D $(Fe\text{-}Mg)^{cpx\text{-}liq} = 0.27 \pm 0.02$, while in sample 3028, $K_D = 0.29 \pm 0.01$. These values are well within the K_D $(Fe\text{-}Mg)^{cpx\text{-}liq}$ values of 0.29 ± 0.08 proposed by Putirka (2008), suggesting that the crystals are in equilibrium with melt.

Crystal assemblages from the analyzed samples reveal no discernable pattern with regard to sample location on the Galema range. Small groupings of samples with similar crystal assemblages are present; however, these small groups lie in close proximity (<5 km) to samples with a dissimilar assemblage. It is unclear if this is an artifact of sample availability or perhaps magmatic processes at such scale.

5. DISCUSSION

5.1. Extensional Strain Accommodation by Zones of Focused Magmatic Intrusion

To first-order, dikes are emplaced perpendicular to the orientation of the least compressive stress (σ_3) (Rubin and Pollard, 1988; Rubin, 1990; Parsons and Thompson, 1991; Rubin, 1992). In rifting environments, the orientation of the least compressive stress is in the direction of the extensional strain imposed on the lithosphere. If this intruded magma is sourced from a location other than the host rock (i.e., not a result of partial melting of the crust) and is allowed to remain in the host rock through magma cooling and dike freezing, the result is an increase of the volume of the host rock (Parsons and Thompson, 1991). In this way, magmatic intrusion accommodates extensional strain. The rapid emplacement of dikes can accommodate up to millennia worth of accumulated strain within the host rock (Parsons and Thompson, 1991). The depth where magma stalls on ascent and forms magma chambers coincides with depths where lithospheric strain accommodation occurs. Locations where magma is emplaced perpendicular to the direction of least principal compressive stress (σ_3), such as areas experiencing lithospheric extension, indicate areas where the crust may accommodate extensional strain aseismically (Corti et al., 2003). Thus, an estimate of the architecture of a magmatic plumbing system and the depths at which magma accumulates can constrain where and how strain is accommodated in the lithosphere in areas of extensional tectonics.

The stalling of a magma on ascent is testable through the study of its major-element geochemistry (e.g., Peccerillo et al., 2003; Rooney, 2010; Trua et al., 1999). The depth at which a magma stalls in the lithosphere, in part, controls the phases that form from that magma, thereby influencing the composition of the phase and residual magma from which the phase fractionates (Green and Ringwood, 1967; Green, 1969; O'Hara, 1968; Thompson, 1972; Wilson, 1994). Previous studies within the region have shown that deeper dike stalling depths resulted in greater stability of clinopyroxene, in contrast to shallower conditions where olivine and plagioclase dominate the

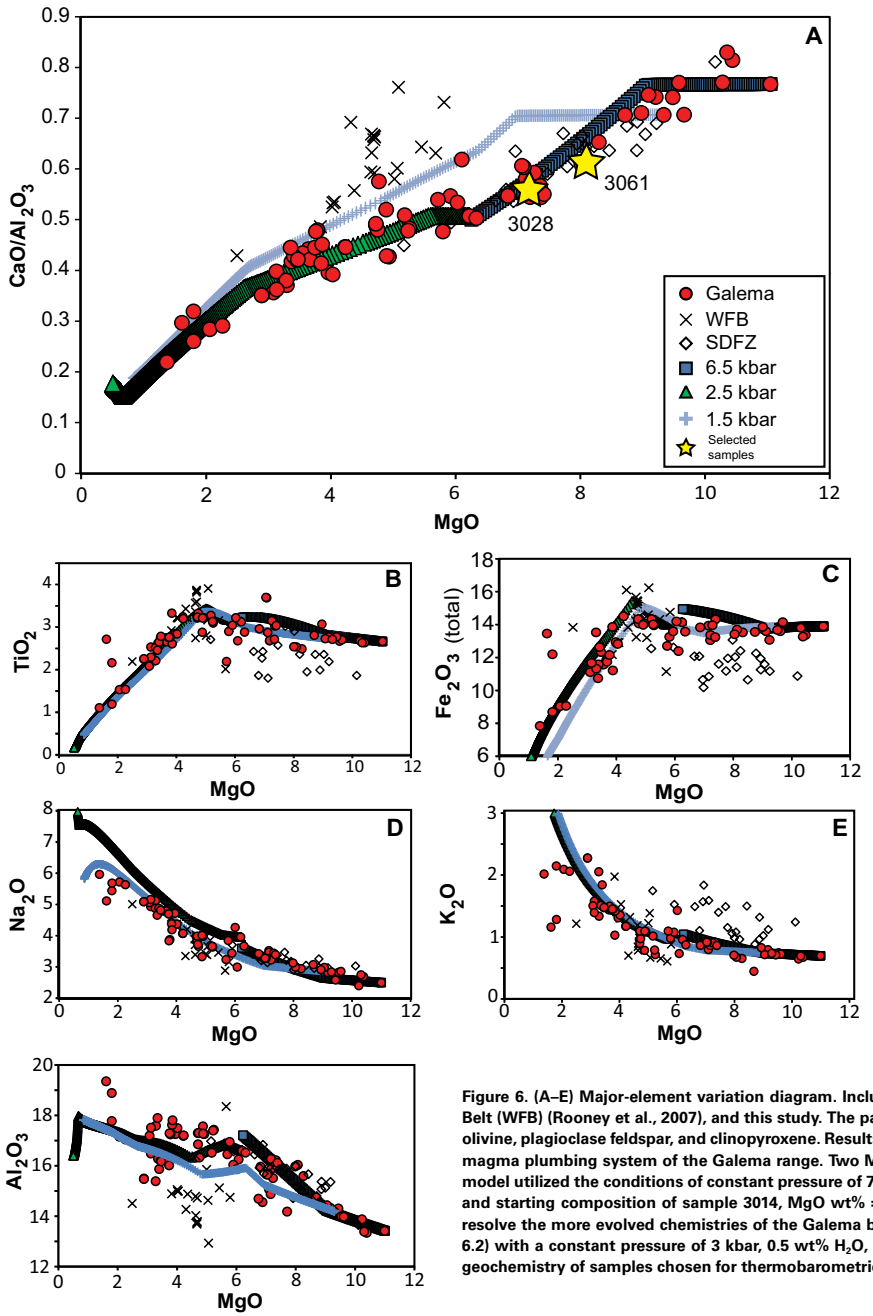

fractionating assemblages, illustrating the use of major-element geochemical analysis in the interpretation of the architecture of a magmatic plumbing system (Peccerillo et al., 2003; Rooney et al., 2007; Rooney et al., 2005; Trua et al., 1999).

5.2. Characterization of the Mafic Magmatic Plumbing System of the Galema Range

5.2.1. MELTS Modeling

To constrain the depths of magma stalling of the Galema range, and thereby establish where extensional strain is being accommodated in the lithosphere, thermodynamic modeling of the crystal fractionation sequence was performed using Excel-MELTS (Asimow and Ghiorso, 1998; Ghiorso and Sack, 1995; Gualda and Ghiorso, 2015). An initial composition for modeling was chosen as the most primitive sample from our data suite (sample 3014, MgO wt% = 11.00) (Fig. 6). Multiple models were run utilizing this initial composition with varying pressures (10 kbar–2 kbar), water contents (0%–5%), and fO_2 (QFM ± 1). Utilizing a constant pressure of 7 kbar, 1 wt% H_2O, and fO_2 value of QFM, with temperature decreasing continuously from 1350 °C, the modeled evolution of this initial composition was found to fit the observed data above ~6.1 wt% MgO in major-element variation diagrams (Fig. 6). At 7 kbar, the MELTS model predicts minor olivine to begin fractionating at 1307 °C (10.98 wt% MgO). The dominant fractionating crystal phase of the model at this pressure is clinopyroxene, which begins fractionating at 1250 °C (9.01 wt% MgO) and continues to where the model deviates from the data at ~6.1 wt% MgO (Fig. 6). Below ~6.1 wt% MgO, the model with these initial conditions deviates significantly from the observed data when plotted in major-element variation diagrams. To resolve this deviation from the observed data, a second model was created, utilizing a starting composition of ~6 wt% MgO (i.e., sample 3016, MgO wt% = 6.20) (Fig. 6). At a constant pressure of 3 kbar, 0.5 wt% H_2O, fO_2 at QFM, and continuous decreasing temperature from 1200 °C, the results of the model fit the observed data with a compositional range of ~1.3 to ~6.1 wt% MgO (Fig. 6). The 3 kbar model predicts that olivine will begin fractionating at 1181 °C (6.21 wt% MgO). At 1158 °C (5.62 wt% MgO), the MELTS model predicts the dominant fractionating crystal phase to be plagioclase, which continues

Figure 6. (A–E) Major-element variation diagram. Included are data from the Silti-Debre Zeyit Fault Zone (SDFZ) (Rooney et al., 2005), the Wonji Fault Belt (WFB) (Rooney et al., 2007), and this study. The patterns observed are consistent with fractionation of the observed mineral assemblages including olivine, plagioclase feldspar, and clinopyroxene. Results of MELTS modeling have been plotted with two trends showing the polybaric architecture of the magma plumbing system of the Galema range. Two MELTS models were applied to fully resolve the chemistry of the Galema basalts. The first MELTS model utilized the conditions of constant pressure of 7 kbar, 1 wt% H_2O, and fO_2 value of 0 QFM with temperature decreasing continuously from 1350 °C and starting composition of sample 3014, MgO wt% = 11.00. This model only resolved the chemistry of the Galema basalts above ~6.1 wt% MgO. To resolve the more evolved chemistries of the Galema basalts, a second model was applied utilizing a starting composition of sample 3016 (MgO wt% = 6.2) with a constant pressure of 3 kbar, 0.5 wt% H_2O, fO_2 at QFM, and continuous decreasing temperature from 1200 °C. (A) Stars indicate whole-rock geochemistry of samples chosen for thermobarometric calculations.

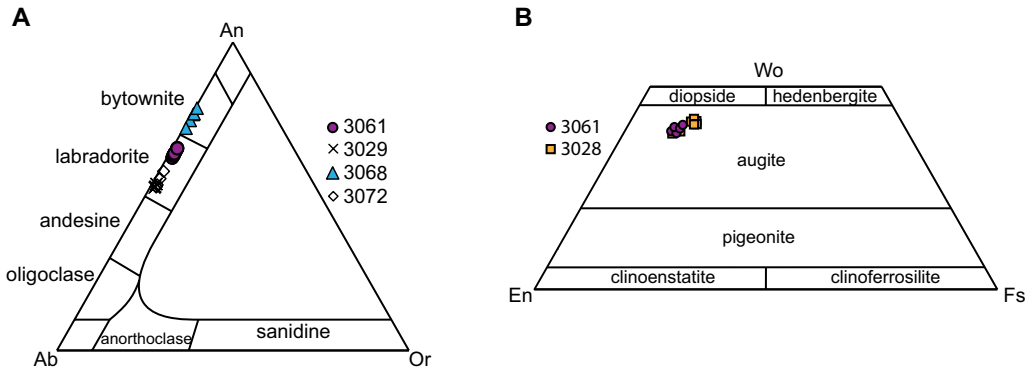

Figure 7. Classification of plagioclase (A) and clinopyroxene (B) phenocrysts from the samples in this study determined through the use of in situ laser ablation–inductively coupled plasma–mass spectrometry (LA-ICP-MS) analysis. See text for sample selection criteria and methods.

fractionating through the end of the model. Minor amounts of spinel will begin fractionating at 1133 °C (4.53 wt% MgO). Minor clinopyroxene does fractionate in the model at this pressure, but plagioclase is clearly fractionating in greater proportion.

The results of the MELTS model agree with the variation diagrams and petrography of the Galema basalts. The 7 kbar model predicts the primary crystalizing phase to be olivine at 10.98 wt% MgO, while the variation diagrams show that olivine is the primary crystalizing phase above ~9 wt% MgO (Fig. 6). This is in agreement with the petrography of samples in that compositional range (Fig. 3). The MELTS model predicts that clinopyroxene should fractionate at 9.01 wt% MgO at 7 kbar, in agreement with the slope of the CaO/Al_2O_3 versus MgO variation diagram in that compositional range (Fig. 6). A subset of samples from compositional range of ~7 to ~8 wt% MgO also displays clinopyroxene as a member of the phenocryst population (Fig. 3). The 3 kbar MELTS model predicts the primary fractionating crystal phase to be plagioclase at ~5.62 wt% MgO, which is in agreement with the CaO/Al_2O_3 versus MgO variation diagram in that compositional range (Fig. 6). The petrography of samples from this compositional range also shows plagioclase as the dominant crystal phase (Fig. 3). The 3 kbar MELTS model predicts spinel fractionating at 4.53 wt% MgO, consistent with the Fe_2O_3 versus MgO variation diagram (Fig. 6) and the occurrence of oxide phases in the petrography (Fig. 3).

Spinel and plagioclase exist in the petrography of the basalts of the Galema range for compositions above ~5.62 wt% MgO, which is not accounted for in the deeper MELTS model (Fig. 6). The presence of these phases may be the result of the shallower fractionation, subsequent to the initial stages where clinopyroxene was dominant at greater depths.

The results of these thermodynamic models are thus consistent with the existence of a polybaric fractionation system, which is centered at 25 and 11km depth (Fig. 8). The modeled pressures of fractionation, when correlated with the suite of samples analyzed, show no discernable correlation with their locations on the Galema range (Fig. 1C).

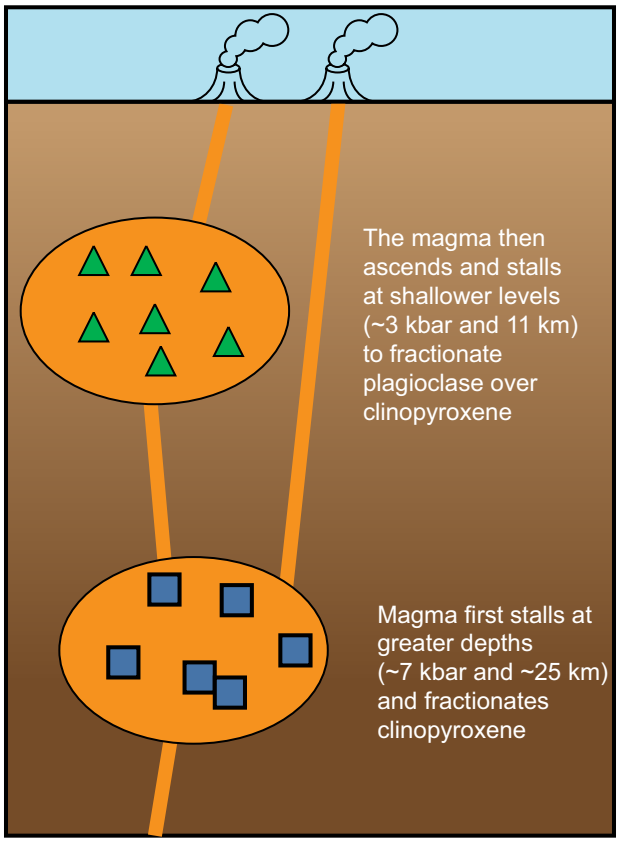

Figure 8. Cartoon depicting the magma plumbing system of the Galema range as indicated by our analysis. Figure not to scale.

5.2.2. Thermobarometry

To ascertain the pressures of fractional crystallization, and to validate the Excel-MELTS model of magmatic evolution, the in situ geochemical analysis of the crystal phases of the Galema range was applied to clinopyroxene-melt thermobarometry calculations (Nimis, 1995). The samples were chosen based upon the MgO compositional range and the availability of analytically suitable clinopyroxene crystals. Liquid compositions for the selected samples were estimated using the whole-rock geochemical data for sample 3028 (60% groundmass) and 3061 (25% groundmass) following the methodology of Bédard (2014), Putirka (2008), and Putirka et al. (2003). The water content (0.1–1 wt%) for the magmas in the thermobarometry calculations were estimated based on the H_2O compositions determined in the MELTS modeling. The thermobarometric calculations determined that samples 3061 and 3028 fractionated at pressures of 6.7–8.6 kbar (24.4 km to 31.3 km depth) (Fig. 9). These calculations are within ±2.0 kbar of the pressures determined in the MELTS models (Fig. 6).

While plagioclase mineral data were collected (Supplemental Tables [footnote 1]), these data were not used in thermobarometric calculations. Plagioclase-liquid thermobarometers have large errors associated with their pressure estimates, with some as high as ±3 kbar (Putirka, 2008). These estimates were not useful for our analysis of the magmatic plumbing system of the Galema range.

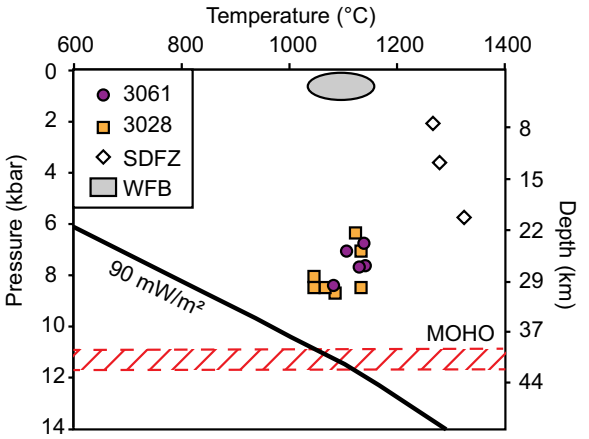

Figure 9. Pressure-temperature chart of clinopyroxene-liquid thermobarometric calculations indicating that Galema magmas fractionated at greater pressure and depth than rift axial and rift marginal magmas. Pressure calculations based on Nimis (1995) and temperature calculations based on Nimis and Taylor (2000). Additional data from Rooney et al. (2005) and Rooney et al. (2007). Moho depth estimates from Keranen et al. (2009). Geotherm estimate from Hasterok and Chapman (2011). SDFZ—Silti-Debre Zeyit Fault Zone; WFB—Wonji Fault Belt.

5.2.3. Geophysical Constraints

Geophysical observations of the lithosphere of the MER show regions of higher P-wave velocities (V_p) in the crust at 10 km beneath the surface expressions of the WFB, SDFZ, and the Galema range (Keranen et al., 2004; Rooney et al., 2014) (Fig. 10A). This higher V_p indicates the existence of higher density material, which is consistent with a considerable volume of solidified, mafic material (interpreted to be gabbroic in composition) that was intruded into the lithosphere (e.g, Keranen et al., 2004; Mahatsente et al., 1999). The differences in magnitude of V_p between the Galema range, WFB, and the SDFZ may be due to differences in the volume of higher density material stored in the lithosphere between each location. This depth at which higher V_p occurs beneath the Galema range is consistent with the results of our MELTS modeling and thermobarometric calculations. This correlation may be evidence of cooled mafic material at these depths, resulting from stalled magmatic intrusion similar to processes observed in the WFB and SDFZ (Keranen et al., 2004; Rooney et al., 2005). Residual gravity measurements are entirely consistent with the seismic velocity anomalies. Specifically, the gravity data show a distinct negative residual gravity across the entire rift. Outside the rift, there is typically no significant anomaly, with the exception of the Galema range on the eastern plateau. The anomaly beneath the Galema range has been previously interpreted to be the result of silicic flows (Mahatsente et al., 1999); however, this interpretation was not based upon field data. The magnitude of this gravity anomaly is related to the amount and density of material within the crust and does not offer a unique solution to the observations.

5.3. Extensional Strain Accommodation by Focused Magmatic Intrusion within the MER

Recent activity in Afar indicates that extensional strain is accommodated by focused magmatic intrusion within polybaric magmatic plumbing systems. Bimodal chemistry of magmatic products within the Dabbahu magmatic segment in Afar has been attributed to polybaric fractionation resulting from multiple depths of magma storage, which is also in agreement with geophysical studies (Ayele et al., 2009; Belachew et al., 2011; Field et al., 2012; Hammond, 2014; Wright et al., 2012). Zones of focused magmatic intrusion are also found in the MER in the WFB and SDFZ. Geophysical measurements show a volume of dense, intruded material within the lithosphere at the SDFZ (Keranen et al., 2004). Geochemical analyses of the magmatic products of the SDFZ indicate that the magmas were derived from sublithospheric depths (Rooney et al., 2005). The intruded material was introduced into the crust adding volume to the lithosphere at the SDFZ, indicating that the magmatism of the SDFZ represents accommodation of strain through focused magmatic intrusion.

Similarly, the WFB in the CMER plausibly represents an area of extensional strain accommodation by focused magmatic intrusion. Intruded material beneath the WFB, which added volume to the lithosphere, has been observed in

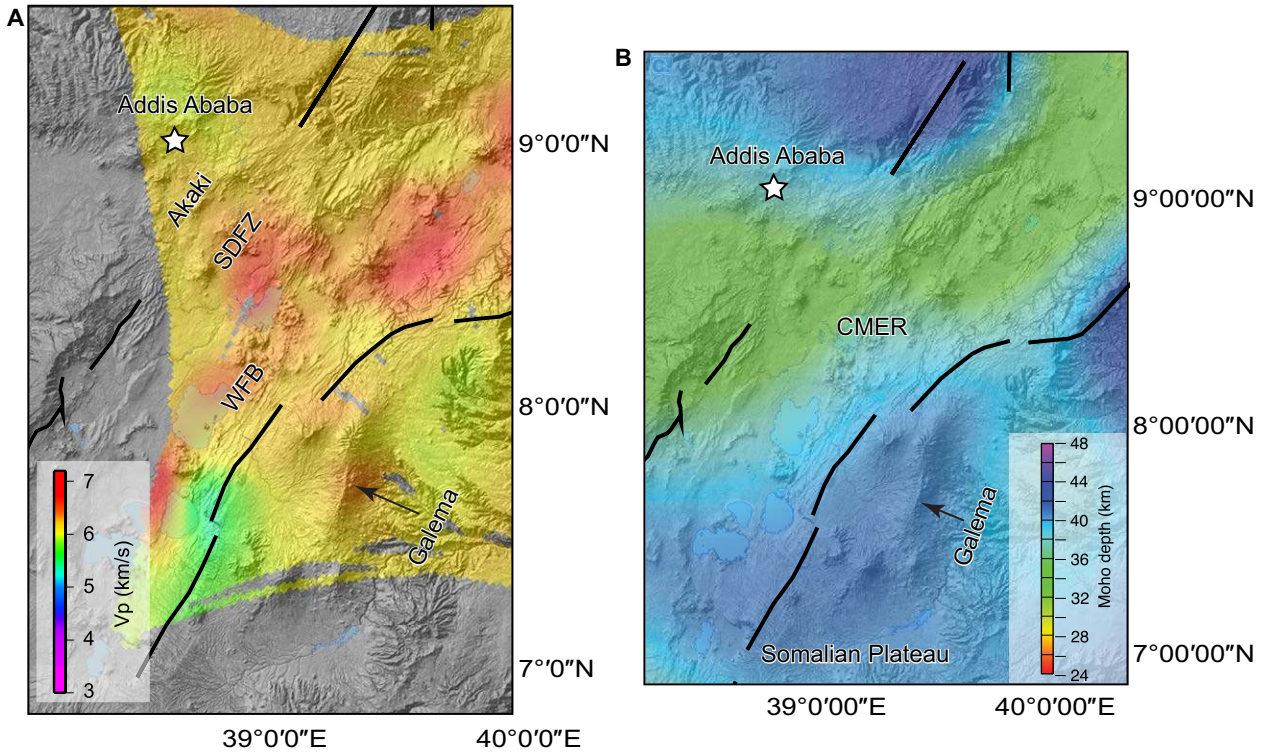

Figure 10. (A) Depth slice at 10 km for V_p in the Central Main Ethiopian Rift (CMER), indicating higher velocities beneath the Galema range, consistent with the presence of solidified mafic material with greater density at depth. Modified from Keranen et al. (2004) and Rooney et al. (2014). (B) Moho depth in the Central Main Ethiopian Rift (CMER), indicating a region of deeper Moho beneath location of the Galema range on the Southeastern Ethiopian Plateau in comparison to Moho depth of areas of focused magmatic activity within the rift valley. The deeper Moho beneath the plateau is an indication of less lithospheric stretching and thinning. Modified from Keranen et al. (2009) and Rooney et al. (2014). SDFZ—Silti-Debre Zeyit Fault Zone; WFB—Wonji Fault Belt.

geophysical measurements (e.g., Bastow et al., 2008; Biggs et al., 2011; Keir et al., 2011; Keir et al., 2015; Keranen et al., 2004; Kim et al., 2012; Rooney et al., 2007). Seismic anisotropy indicates the structure of these intrusions to be vertical dikes aligned in the orientation perpendicular to the extensional stress field affecting the MER (Keir et al., 2005; Kendall et al., 2006). These dikes are not derived from partial melting of the lithosphere, again requiring added volume to the crust (Rooney et al., 2007; Rooney et al., 2011). The WFB thus represents an area of magmatic strain accommodation.

As noted previously, the Galema range displays a similar morphology to the Quaternary zones of focused intrusion within the MER. The morphological similarities between the Galema range and areas of focused magmatism within the rift (e.g., dikes aligned perpendicular to the σ_3 induced by the extensional stress field) suggest that the Galema range also magmatically accommodated strain, but intriguingly, exists outside the rift proper.

The polybaric fractionation system of the Galema range is also consistent with the architecture of the magma plumbing system of the WFB. Thermodynamic modeling, petrographic modeling, and thermobarometric calculations have shown that the WFB consists of a polybaric fractionation system at deep crustal levels before magma ascends to consistently shallow levels within the crust (Rooney et al., 2005; Rooney et al., 2007; Rooney et al., 2011; Trua et al., 1999). The magmas of the WFB have been interpreted, through clinopyroxene thermobarometry, as having crystallization pressures of 0.1 kbar to 5.0 kbar (Rooney et al., 2007)—a narrower and shallower range of fractionation depths than the magmas of the Galema range.

The thermobarometric calculations of the Galema range indicate greater pressures of magma stalling and fractionation in comparison to those found at the WFB. These pressures are more consistent with those determined from analyses of the SDFZ. The SDFZ displays geochemical evidence of increased

fractionation of clinopyroxene over plagioclase in its magmas, suggesting deeper levels of fractionation than at the WFB (e.g., Green and Ringwood, 1967; Rooney et al., 2007; Rooney et al., 2005). Similarly, thermobarometric estimates derived from host lavas within the SDFZ indicate fractionation pressures over a range from 2.0 kbar to 5.6 kbar (Rooney et al., 2005). This increased depth of magma stalling for the less mature magmatic plumbing system of the SDFZ is more similar to the Galema range. These observations indicate a greater similarity in magmatic processes between the Galema range and the SDFZ in comparison to the WFB.

5.4. Factors Controlling the Depth of Magmatic Stalling in Extensional Settings

Thermal modification of the base of the lithosphere allows for magma to intrude and begin fluxing into the affected areas (Havlin et al., 2013). This thermal modification allows for subsequent dikes to intrude further before freezing, broadly modifying the lithosphere in such a way as to allow diking and magma ascent to proceed (Bastow and Keir, 2011; Bialas et al., 2010; Daniels et al., 2014; Havlin et al., 2013). Once in the lithosphere, the depth at which a magma may stall is controlled by how the buoyancy forces of the magma interact with density contrasts of the lithosphere (Menand, 2011).

Buoyancy forces affecting a dike within the lithosphere depend on the availability and amount of magma generated (Parsons and Thompson, 1991). Buoyant magma will ascend to levels within the lithosphere where density differences are equal to the magma overpressure, which is generated by the buoyancy forces (Rubin, 1990). However, in a persistent rift zone, the constant extensional stress in the lithosphere is large enough to offset the stress state that results from lithospheric density differences (Rubin, 1990). If the extensional stress field increases during dike ascension, but magma flux remains constant, the magma overpressure is essentially cancelled, and the dike is trapped at depth. Extension reduces the horizontal stress perpendicular to the rift zone (σ_3), allowing dikes to increase in width, but decreases their chance for ascent when the extensional stress field returns to normal (Rubin, 1990). If magma flux and resultant magma overpressure increased after such an event, the dike would again be allowed to ascend, but in a wider, more well developed conduit.

Magma flux into the lithosphere determines the development of a rift magmatic plumbing system. Greater available magma volume is necessary to form larger dikes, which may traverse the crust to shallow levels (Rooney et al., 2014). A reduced magma flux into the lithosphere would create a more complex magmatic plumbing system because smaller dikes would have difficulty ascending directly to the surface due to reduced thermal weakening of the lithosphere (Bialas et al., 2010; Buck, 2004; Havlin et al., 2013). The less mature magmatic plumbing system of the Galema range, in comparison to the WFB, may be due to an overall decreased magma flux into the lithosphere resulting from both the average extent and rate of lithospheric stretching and thinning. This reduced magma flux would also inhibit the ascension of any dikes trapped at depth due to a temporary increase in the local stress field.

5.5. Lithospheric Extension and Magma Generation

As the lithosphere thins, the underlying asthenosphere must ascend to compensate partially for this reduced thickness, generating an increasing melt (Langmuir and Forsyth, 2007). Increased extension rate also increases the amount of adiabatic melting of the asthenosphere and can therefore increase magma flux into the lithosphere (Langmuir and Forsyth, 2007).

With progressive lithospheric thinning, the depth of melting of the asthenosphere shallows as the lithospheric cap is reduced, and adiabatic melting can occur at decreased depth (Rooney, 2010; Wang et al., 2002). Stretching of the lithosphere manifests as an overall thinning of the plate, resulting in a shallowing of both lithosphere-asthenosphere boundary (LAB) and the Moho. Active source seismic studies within the MER show a Moho depth of ~32–36 km, but beneath the relatively less stretched Southeastern Ethiopian Plateau, upon which the Galema range lies, the Moho is at a depth of ~42–46 km (Keranen et al., 2009; Rooney et al., 2014) (Fig. 10B). Given this increased Moho depth, we anticipate a deeper melting column beneath the Galema range (which is controlled by the depth of the LAB).

An examination of the melting depth of the magmas of the Galema range reveals depths greater than those at the WFB. Variation of SiO_2 versus FeO* for Galema range lavas (corrected for olivine fractionation using the PRIMELT3 MEGA modeling suite; Herzberg and Asimow, 2015) exhibits a distinct grouping displaying higher FeO* content than experimentally derived melts of fertile mantle peridotite at a pressure of ~25–30 kbar (Baker and Stolper, 1994; Furman et al., 2006; Kushiro, 1996) (Fig. 11). The grouping of the Galema range lavas at high FeO* also exceeds lavas from the adjacent MER, e.g., the WFB and Akaki (Rooney et al., 2007; Rooney et al., 2014) and suggests a source melt for the Galema basalts at pressures greater than ~30 kbar (~110 km depth), deeper than the interpreted melting depths of the WFB and Akaki (~73 km depth) (Fig. 11A). Compositions from the Galema range do not plot along the same trend as other areas of focused magmatic activity within the MER on an olivine-plagioclase-quartz ternary diagram. While the compositions of the other areas of focused magmatic activity (WFB, SDFZ, and Akai) plot along experimentally derived boundary curves for the 3-phase saturated liquid at 30 kbar (Hirose and Kushiro, 1993; Walker et al., 1979), Galema range compositions plot in a region that may indicate a higher melting pressure (Fig. 11B). We suggest that the source melt of the Galema range was generated beneath thicker lithosphere in comparison to melts within the MER.

5.6. Model for the Development of Extension along the Asela-Sire Border Faults

5.6.1. Formation of the Asela-Sire Border Faults

Rifting initially manifests as faulting and progresses toward the development of connected half grabens (Ebinger, 2005). The classic continental rift shape of a downthrown valley floor and steep, high-angle border faults de-

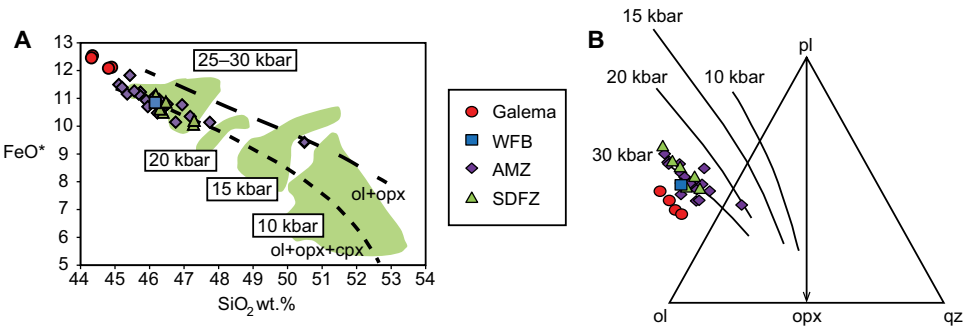

Figure 11. (A) FeO* versus SiO diagram, after Furman et al. (2006) and Baker and Stolper (1994), suggesting that the source melt of the material of the Galema range was generated at ~30 kbar pressure. Iron content for samples was converted to FeO total and corrected to primary composition using PRIMELT3MEGA (Herzberg and Asimow, 2015) to obtain FeO*. Only samples with Mg# >62 were used. Additional sample data from Furman et al. (2006); Rooney et al. (2014); and Rooney et al. (2005). (B) Olivine-plagioclase-quartz (ol-pl-qz) ternary diagram, along with boundary curves plotted experimentally for the 3-phase saturated liquids at different pressures (after Hirose and Kushiro, 1993; Walker et al., 1979) showing that samples from the Galema range plot away from the 30 kbar pressure line, indicating greater pressure of melt generation. Samples were corrected to primary composition using PRIMELT3MEGA (Herzberg and Asimow, 2015) before computation of components. Only samples with Mg# >62 were used. Additional sample data from Furman et al. (2006); Rooney et al. (2014); and Rooney et al. (2005). Opx—orthopyroxene; cpx—clinopyroxene; SDFZ—Silti-Debre Zeyit Fault Zone; WFB—Wonji Fault Belt; AMZ—Akaki magmatic zone.

velop and progressive faulting becomes more focused within the rift valley (Corti, 2012; Corti et al., 2004; Maccaferri et al., 2014; Wolfenden et al., 2005). These faults have accommodated strain since their formation, though it is difficult to ascertain if this accommodation of strain was of a constant magnitude throughout their history.

5.6.2. Melt Generation, Migration, and Initiation of Magmatic Intrusion at the Galema Range

Thinning of the lithosphere occurs in response to the extensional forces induced during continental rifting. Recent estimates indicate that within the MER, both the crust and lithosphere are thinned beneath the rift valley (Bastow and Keir, 2011; Keir et al., 2015; Keranen et al., 2009; Rooney et al., 2014). This thinning of the lithosphere results in decompression and consequent melting of the underlying asthenosphere, generating the melt necessary for continental rifting processes to occur (Ebinger, 2005; Ebinger and Casey, 2001; Ebinger and Sleep, 1998; Langmuir and Forsyth, 2007; McKenzie and Bickle, 1988). As magma began to intrude at the base of the lithosphere, perpendicular to the σ_3 generated by the regional extensional stress, the thermal gradient rose, broadly modifying the lithosphere in such a way as to allow diking and magma ascent to proceed (Bastow and Keir, 2011; Bialas et al., 2010; Daniels et al., 2014; Havlin et al., 2013).

Following the generation of melt beneath the rift margin, subsidence of the half grabens forced magma laterally along the base of the crust to outside of the border faults (Corti et al., 2003; Corti et al., 2004; Maccaferri et al., 2014). As this melt was relocated to beneath the Southeastern Ethiopian Plateau, it raised the thermal gradient and assisted in the thermomechanical modification of the lithosphere at that location (Bastow and Keir, 2011; Bialas et al., 2010; Daniels et al., 2014; Havlin et al., 2013) (Fig. 12) This modification facilitated subsequent magmatic intrusion, which ascended to form the Galema range. Additionally, the thermal modification induced by magmatic intrusion would have the effect of reducing lithospheric strength to a degree that would make strain accommodation by faulting unfavorable within the extensional stress field (Buck, 2004). Thus, activity of the nearby Asela-Sire Border Fault would have ceased or been reduced during these events. The local stress field and presence of preexisting lithospheric heterogeneities within the crust, at the time of the formation of the Galema range, dictated the pathways of ascent and determined the location and morphology of the range (Mazzarini et al., 2013; Rooney et al., 2014). Magmatic intrusion through preexisting lithospheric weaknesses will still result in extensional strain accommodation through the addition of volume to the crust if the intruded material remains within the host rock and is not sourced from the host rock itself.

5.6.3. Cessation of Magmatism in the Galema Range

After the formation of the Galema range, magmatism in this off-rift location ceased due to several possible processes related to either continued extension or reduced magma supply or both. A temporary reduction in the extension rate would lead to a reduction in adiabatic melting of the asthenosphere, limiting the amount of magma available to flux into the lithosphere. This reduced magma supply would have the effect of decreasing the magma overpressure in ascending dikes, allowing them to become trapped at depths where this pressure equals the density-controlled stress within the surrounding lithosphere. If extension and resultant magma production continued to be diminished for a long enough period, the dikes that had previously ascended into the lithosphere would freeze, effectively ending magmatic activity.

As the lithosphere continued to deform and thin along the rift axis, magmatism shifted toward more focused activity along the axis due to increased magma flux created by adiabatic melting in the newly thinned areas (Ebinger, 2005; Morton et al., 1979). Magmatism may also shift location due to a change in the topography at the base of the lithosphere (as a result of progressive thinning), which channels melt material toward the axis (Corti, 2012; Keir et al., 2015). While the shift in magmatic activity toward the rift axis may be due to a change in topography at the base of the lithosphere, we modify this model to include magmatic intrusion of the Galema range dikes and the consequent unavoidable thermomechanical modification of the lithosphere (Bastow and Keir, 2011; Bialas et al., 2010; Buck, 2004; Daniels et al., 2014; Havlin et al., 2013).

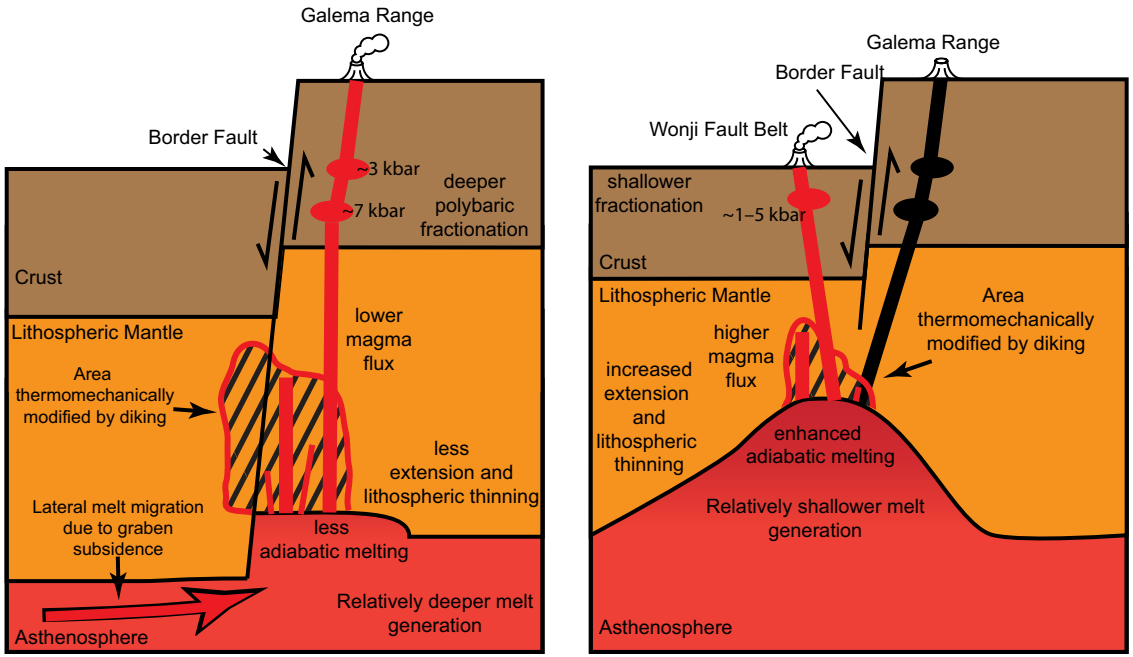

Figure 12. Cartoon showing the hypothesized formation of the Galema range and subsequent formation of the Wonji Fault Belt (WFB) on the eastern rift margin. Initial activity of the Galema range generated thermomechanical modification of the lithosphere resulting from vertical diking and ascending magma. This area of modified lithosphere facilitated the ascent of the magma that would form the WFB. Following this, a reduction or pause in the extension resulted in less magma available to flux into the lithosphere. This reduction in magma supply reduced the magma overpressure necessary for dike ascension and caused a cessation of magmatism at the Galema range. Continued extension progressively thinned the lithosphere within the rift, generating a greater adiabatic melt fraction from shallower depths. The increased melt resulted in an increased magma flux into the lithosphere, allowing for the development of a more well-developed magma plumbing system at the younger WFB. This more well developed magma plumbing system allowed the WFB to become the dominant location of magmatic strain accommodation within the rift as a result of the thermomechanical modification of the earlier diking beneath the Galema range. Figure not to scale.

5.6.4. Initiation of Magmatism of the WFB

Lithospheric thinning associated with continued extension generated an increased melt fraction at shallower depths (Langmuir and Forsyth, 2007; McKenzie and Bickle, 1988). The magma generated during this more advanced state of extension intruded the lithosphere at the same broad location, which was thermomechanically modified by the previous activity of the Galema range.

The greater melt fraction increased the magma flux into the lithosphere, allowing for the formation of larger dikes. These larger dikes would be able to more easily ascend to the surface, forming more well developed magmatic plumbing system with shallower levels of fractionation, as observed at the WFB (Rooney et al., 2014) (Fig. 12). Greater melt production would allow for an increase in the amount of magmatic material erupted, increasing surface topography and simultaneously reducing the extensional stress at the bottom of the lithospheric plate through magma injection. This dynamic allows magma to ascend to shallower levels before stalling (Behn et al., 2006).

As a continental rift evolves, magmatism is influenced less by preexisting lithospheric structures and more by the lithospheric strain profile due to the thermal modification of the lithosphere (Isola et al., 2014; Robertson et al., 2016). Magmatism became the dominant form of strain accommodation in the WFB as a result of the enhancement of the magmatic plumbing system assisted by, among other processes, the earlier focused magmatism of the Galema range. Furthermore, this suggests that magmatic strain accommodation does not linearly migrate toward the rift axis during rift evolution and may in fact be more distributed and episodic.

5.7. Broader Impacts

During the early stages of continental rifting, extensional strain is accommodated through faulting and stretching of the lithosphere, resulting in the formation of the high-angle border faults that will define the rift. Following this, magmatic intrusion begins to accommodate extensional strain, which should migrate and focus along the rift axis (Wolfenden et al., 2005). Recent work has suggested that strain accommodation in the Afar region via focused magmatic intrusion did not occur until very recently and that prior to this, the only expression of magmatic activity was the emplacement of large-scale flood basalts (Stab et al., 2015). These areas of focused magmatic intrusion may represent the organization of magmatic strain accommodation organizing into axial segments (Medynski et al., 2015). The Galema range may represent an intermediate stage of continental rifting, occurring after the formation of the rift-border faults but before the organization of axial magmatic segments. This

intermediate stage is characterized by pulsed accommodation of extensional strain by focused magmatic intrusion outside the rift proper and accommodation of extensional strain by faulting and stretching of the lithosphere during periods between magmatic intrusions.

6. CONCLUSIONS

The Galema range, which is located on the Southeastern Ethiopian Plateau adjacent to the rift margin, is a zone of focused dike intrusion that displays morphological similarities to zones of focused magmatic intrusion within the Main Ethiopian Rift. Our results demonstrate that the depths of stalling of the mafic magmas of the Galema range are deeper than those at the WFB, consistent with a less developed magma plumbing system for the Galema range. We find that magma generation beneath the Galema range occurs at greater depths than beneath the WFB, indicating that the lithosphere had undergone relatively less extension in comparison to the modern rift. On the basis of these observations, and existing geodynamic constraints, we propose the following model explaining the origin of off-axis zones of focused intrusion: (1) the initial development of rift-border faults controlled the migration of melt into the lithospheric mantle. The transit of the melt through the crust was controlled, in part, by the establishment of a horizontal axis of least compressive stress during graben formation and thereby facilitating rift adjacent volcanism; and (2) with continued rift evolution, the transit of melt through the lithospheric mantle occurred along the same pathways established during the earlier rift-adjacent volcanism enhancing magmatism along one rift margin. However, variations in the amount of magma production and resultant magma overpressure in ascending dikes may have allowed for the eruption of within-rift zones of focused intrusion.

We propose that the Galema range represents an intermediate stage of continental rift evolution, occurring after the formation of the rift-border faults but before the formation of axial magmatic segments. In this hybrid rifting model, strain is accommodated by oscillations between both the rift-border faults and areas of focused magmatic intrusion. However, the amount of strain partitioned between each mechanism and the timing are not yet resolved. These findings have implications for the initial development of zones of focused magmatic intrusion within rifts. In particular, this work demonstrates that it is possible to have multiple periods of extension being accommodated through focused magmatic intrusion or displacement of faults along a single margin. These observations will need to be incorporated into ongoing debates about the timing of initiation of magma-facilitated extension (Stab et al., 2015; Wolfenden et al., 2005).

ACKNOWLEDGMENTS

This work was supported by the National Aeronautics and Space Administration Planetary Geology and Geophysics Program (grant 10-PGG10-006). We would like to thank Giacomo Corti and the anonymous reviewer for their comments, which have greatly improved this work, and Shanaka de Silva for careful editorial handling.

REFERENCES CITED

Abebe, T., Mazzarini, F., Innocenti, F., and Manetti, P., 1998, The Yerer-Tullu Wellel volcanotectonic lineament: A transtensional structure in central Ethiopia and the associated magmatic activity: Journal of African Earth Sciences, v. 26, p. 135–150, https://doi.org/10.1016/S0899-5362(97)00141-3.

Abebe, B., Acocella, V., Korme, T., and Ayalew, D., 2007, Quaternary faulting and volcanism in the Main Ethiopian Rift: Journal of African Earth Sciences, v. 48, p. 115–124, https://doi.org/10.1016/j.jafrearsci.2006.10.005.

Abebe, T., Balestrieri, M.L., and Bigazzi, G., 2010, The central Main Ethiopian rift is younger than 8 Ma: confirmation through apatite fission-track thermochronology: Terra Nova, v. 22, p. 470–476, https://doi.org/10.1111/j.1365-3121.2010.00968.x.

Acocella, V., Korme, T., and Salvini, F., 2003, Formation of normal faults along the axial zone of the Ethiopian Rift: Journal of Structural Geology, v. 25, p. 503–513, https://doi.org/10.1016/S0191-8141(02)00047-0.

Agostini, A., Corti, G., Zeoli, A., and Mulugeta, G., 2009, Evolution, pattern, and partitioning of deformation during oblique continental rifting: Inferences from lithospheric-scale centrifuge models: Geochemistry, Geophysics, Geosystems, v. 10, no. 11, https://doi.org/10.1029/2009GC002676.

Agostini, A., Bonini, M., Corti, G., Sani, F., and Manetti, P., 2011a, Distribution of Quaternary deformation in the central Main Ethiopian Rift, East Africa: Tectonics, v. 30, no. 4, https://doi.org/10.1029/2010TC002833.

Agostini, A., Bonini, M., Corti, G., Sani, F., and Mazzarini, F., 2011b, Fault architecture in the Main Ethiopian Rift and comparison with experimental models: Implications for rift evolution and Nubia-Somalia kinematics: Earth and Planetary Science Letters, v. 301, p. 479–492, https://doi.org/10.1016/j.epsl.2010.11.024.

Asimow, P.D., and Ghiorso, M.S., 1998, Algorithmic modifications extending MELTS to calculate subsolidus phase relations: The American Mineralogist, v. 83, p. 1127–1132, https://doi.org/10.2138/am-1998-9-1022.

Ayele, A., Keir, D., Ebinger, C., Wright, T.J., Stuart, G.W., Buck, W.R., Jacques, E., Ogubazghi, G., and Sholan, J., 2009, September 2005 mega-dike emplacement in the Manda-Harraro nascent oceanic rift (Afar depression): Geophysical Research Letters, v. 36, no. 20, https://doi.org/10.1029/2009GL039605.

Baker, B., 1987, Outline of the petrology of the Kenya rift alkaline province, *in* Fitton, J.G., and Upton, B.G.J., eds., Alkaline Igneous Rocks: Geological Society of London, Special Publications, v. 30, p. 293–311, https://doi.org/10.1144/GSL.SP.1987.030.01.14.

Baker, J., Snee, L., and Menzies, M., 1996, A brief Oligocene period of flood volcanism in Yemen: Implications for the duration and rate of continental flood volcanism at the Afro-Arabian triple junction: Earth and Planetary Science Letters, v. 138, p. 39–55, https://doi.org/10.1016/0012-821X(95)00229-6.

Baker, M.B., and Stolper, E.M., 1994, Determining the composition of high-pressure mantle melts using diamond aggregates: Geochimica et Cosmochimica Acta, v. 58, p. 2811–2827, https://doi.org/10.1016/0016-7037(94)90116-3.

Balestrieri, M.L., Bonini, M., Corti, G., Sani, F., and Philippon, M., 2016, A refinement of the chronology of rift-related faulting in the Broadly Rifted Zone, southern Ethiopia, through apatite fission-track analysis: Tectonophysics, v. 671, p. 42–55, https://doi.org/10.1016/j.tecto.2016.01.012.

Bastow, I.D., and Keir, D., 2011, The protracted development of the continent-ocean transition in Afar: Nature Geoscience, v. 4, p. 248–250, https://doi.org/10.1038/ngeo1095.

Bastow, I.D., Nyblade, A.A., Stuart, G.W., Rooney, T.O., and Benoit, M.H., 2008, Upper mantle seismic structure beneath the Ethiopian hot spot: Rifting at the edge of the African low-velocity anomaly: Geochemistry, Geophysics, Geosystems, v. 9, no. 12, https://doi.org/10.1029/2008GC002107.

Bédard, J.H., 2014, Parameterizations of calcic clinopyroxene—Melt trace element partition coefficients: Geochemistry, Geophysics, Geosystems, v. 15, no. 2, p. 303–336, https://doi.org/10.1002/2013GC005112.

Behn, M.D., Buck, W.R., and Sacks, I.S., 2006, Topographic controls on dike injection in volcanic rift zones: Earth and Planetary Science Letters, v. 246, p. 188–196, https://doi.org/10.1016/j.epsl.2006.04.005.

Belachew, M., Ebinger, C., Coté, D., Keir, D., Rowland, J., Hammond, J., and Ayele, A., 2011, Comparison of dike intrusions in an incipient seafloor-spreading segment in Afar, Ethiopia: Seismicity perspectives: Journal of Geophysical Research. Solid Earth, v. 116, no. 6, https://doi.org/10.1029/2010JB007908.

Bendick, R., McClusky, S., Bilham, R., Asfaw, L., and Klemperer, S., 2006, Distributed Nubia—Somalia relative motion and dike intrusion in the Main Ethiopian Rift: Geophysical Journal International, v. 165, p. 303–310, https://doi.org/10.1111/j.1365-246X.2006.02904.x.

Bialas, R.W., Buck, W.R., and Qin, R., 2010, How much magma is required to rift a continent?: Earth and Planetary Science Letters, v. 292, p. 68–78, https://doi.org/10.1016/j.epsl.2010.01.021.

Biggs, J., Bastow, I.D., Keir, D., and Lewi, E., 2011, Pulses of deformation reveal frequently recurring shallow magmatic activity beneath the Main Ethiopian Rift: Geochemistry, Geophysics, Geosystems, v. 12, no. 9, https://doi.org/10.1029/2011GC003662.

Bilham, R., Bendick, R., Larson, K., Mohr, P., Braun, J., Tesfaye, S., and Asfaw, L., 1999, Secular and tidal strain across the Main Ethiopian Rift: Geophysical Research Letters, v. 26, p. 2789–2792, https://doi.org/10.1029/1998GL005315.

Boccaletti, M., Bonini, M., Mazzuoli, R., Abebe, B., Piccardi, L., and Tortorici, L., 1998, Quaternary oblique extensional tectonics in the Ethiopian Rift (Horn of Africa): Tectonophysics, v. 287, p. 97–116, https://doi.org/10.1016/S0040-1951(98)80063-2.

Bonini, M., Corti, G., Innocenti, F., Manetti, P., Mazzarini, F., Abebe, T., and Pecskay, Z., 2005, Evolution of the Main Ethiopian Rift in the frame of Afar and Kenya rifts propagation: Evolution of the Main Ethiopian Rift: Tectonics, v. 24, https://doi.org/10.1029/2004TC001680.

Buck, W.R., 2004, Consequences of asthenospheric variability on continental rifting, *in* Karner, G.D., Taylor, B., Driscoll, N.W., and Kohlstedt, D.L., eds., Rheology and Deformation of the Lithosphere at Continental Margins: New York, Columbia University Press, p. 1–30.

Buck, W.R., 2006, The role of magma in the development of the Afro-Arabian Rift System, *in* Fitton, J.G., and Upton, B.G.J., eds., Alkaline Igneous Rocks: Geological Society of London, Special Publications, v. 259, p. 43–54, https://doi.org/10.1144/GSL.SP.2006.259.01.05.

Casey, M., Ebinger, C., Keir, D., Gloaguen, R., and Mohamed, F., 2006, Strain accommodation in transitional rifts: Extension by magma intrusion and faulting in Ethiopian rift magmatic segments: Geological Society of London, Special Publications, v. 259, p. 143, https://doi.org/10.1144/GSL.SP.2006.259.01.13.

Corti, G., 2008, Control of rift obliquity on the evolution and segmentation of the main Ethiopian rift: Nature Geoscience, v. 1, p. 258, https://doi.org/10.1038/ngeo160.

Corti, G., 2009, Continental rift evolution: From rift initiation to incipient break-up in the Main Ethiopian Rift, East Africa: Earth-Science Reviews, v. 96, p. 1–53, https://doi.org/10.1016/j.earscirev.2009.06.005.

Corti, G., 2012, Evolution and characteristics of continental rifting: Analog modeling-inspired view and comparison with examples from the East African Rift System: Tectonophysics, v. 522–523, p. 1–33, https://doi.org/10.1016/j.tecto.2011.06.010.

Corti, G., Bonini, M., Conticelli, S., Innocenti, F., Manetti, P., and Sokoutis, D., 2003, Analogue modelling of continental extension: A review focused on the relations between the patterns of deformation and the presence of magma: Earth-Science Reviews, v. 63, p. 169–247, https://doi.org/10.1016/S0012-8252(03)00035-7.

Corti, G., Bonini, M., Sokoutis, D., Innocenti, F., Manetti, P., Cloetingh, S., and Mulugeta, G., 2004, Continental rift architecture and patterns of magma migration: A dynamic analysis based on centrifuge models: Tectonics, v. 23, https://doi.org/10.1029/2003TC001561.

Corti, G., Philippon, M., Sani, F., Keir, D., and Kidane, T., 2013, Re-orientation of the extension direction and pure extensional faulting at oblique rift margins: Comparison between the Main Ethiopian Rift and laboratory experiments: Terra Nova, v. 25, p. 396–404, https://doi.org/10.1111/ter.12049.

Daniels, K.A., Bastow, I.D., Keir, D., Sparks, R.S.J., and Menand, T., 2014, Thermal models of dyke intrusion during development of continent-ocean transition: Earth and Planetary Science Letters, v. 385, p. 145–153, https://doi.org/10.1016/j.epsl.2013.09.018.

Ebinger, C., 2005, Continental break-up: The East African perspective: Astronomy and Geophysics, v. 46, no. 2, p. 2.16–12.21, https://doi.org/10.1111/j.1468-4004.2005.46216.x.

Ebinger, C., and Casey, M., 2001, Continental breakup in magmatic provinces: An Ethiopian example: Geology, v. 29, p. 527–530, https://doi.org/10.1130/0091-7613(2001)029<0527:CBIMPA>2.0.CO;2.

Ebinger, C.J., and Sleep, N., 1998, Cenozoic magmatism throughout east Africa resulting from impact of a single plume: Nature, v. 395, p. 788–791, https://doi.org/10.1038/27417.

Ebinger, C., Yemane, T., Woldegabriel, G., Aronson, J., and Walter, R., 1993, Late Eocene–Recent volcanism and faulting in the southern main Ethiopian rift: Journal of the Geological Society, v. 150, p. 99–108, https://doi.org/10.1144/gsjgs.150.1.0099.

Field, L., Blundy, J., Brooker, R., Wright, T., and Yirgu, G., 2012, Magma storage conditions beneath Dabbahu Volcano (Ethiopia) constrained by petrology, seismicity and satellite geodesy: Bulletin of Volcanology, v. 74, p. 981–1004, https://doi.org/10.1007/s00445-012-0580-6.

Furman, T., Bryce, J., Rooney, T., Hanan, B., Yirgu, G., and Ayalew, D., 2006, Heads and tails: 30 million years of the Afar plume, *in* Fitton, J.G., and Upton, B.G.J., eds., Alkaline Igneous Rocks: Geological Society of London, Special Publications, v. 259, p. 95–119, https://doi.org/10.1144/GSL.SP.2006.259.01.09.

Gasparon, M., Innocenti, F., Manetti, P., Peccerillo, A., and Tsegaye, A., 1993, Genesis of the Pliocene to Recent bimodal mafic-felsic volcanism in the Debre Zeyt area, central Ethiopia: Volcanological and geochemical constraints [and the Middle East]: Journal of African Earth Sciences, v. 17, p. 145–165, https://doi.org/10.1016/0899-5362(93)90032-L.

George, R., and Rogers, N., 2002, Plume dynamics beneath the African plate inferred from the geochemistry of the Tertiary basalts of southern Ethiopia: Contributions to Mineralogy and Petrology, v. 144, p. 286–304, https://doi.org/10.1007/s00410-002-0396-z.

Ghiorso, M.S., and Sack, R.O., 1995, Chemical mass transfer in magmatic processes IV. A revised and internally consistent thermodynamic model for the interpolation and extrapolation of liquid-solid equilibria in magmatic systems at elevated temperatures and pressures: Contributions to Mineralogy and Petrology, v. 119, p. 197–212, https://doi.org/10.1007/BF00307281.

Green, D.H., and Ringwood, A.E., 1967, The genesis of basaltic magmas: Contributions to Mineralogy and Petrology, v. 15, p. 103–190, https://doi.org/10.1007/BF00372052.

Gregory, J.W., 1920, The African rift valleys: The Geographical Journal, v. 56, p. 13–41.

Green, T.H., 1969, High-pressure experimental studies on the origin of anorthosite: Canadian Journal of Earth Sciences, v. 6, p. 427–440, https://doi.org/10.1139/e69-041.

Gregory, J.W., Baker, E.G., Britten, J., Rendle, A.B., Gepp, A., Smith, A.L., Carruthers, J.B., Clarke, C.B., Thomas, O.R., Clark, R., and John, M., 1896, The Great Rift Valley: Being the narrative of a journey to Mount Kenya and Lake Baringo: With some account of the geology, natural history, anthropology and future prospects of British East Africa: London, John Murray, 405 p., https://doi.org/10.5962/bhl.title.12499.

Gualda, G.A.R., and Ghiorso, M.S., 2015, MELTS_Excel: AMicrosoft Excel-based MELTS interface for research and teaching of magma properties and evolution: Geochemistry, Geophysics, Geosystems, v. 16, p. 315–324, https://doi.org/10.1002/2014GC005545.

Hammond, J., 2014, Constraining melt geometries beneath the Afar Depression, Ethiopia from teleseismic receiver functions: The anisotropic H-κ stacking technique: Geochemistry, Geophysics, Geosystems, v. 15, p. 1316–1332, https://doi.org/10.1002/2013GC005186.

Hasterok, D., and Chapman, D., 2011, Heat production and geotherms for the continental lithosphere: Earth and Planetary Science Letters, v. 307, p. 59–70, https://doi.org/10.1016/j.epsl.2011.04.034.

Havlin, C., Parmentier, E.M., and Hirth, G., 2013, Dike propagation driven by melt accumulation at the lithosphere-asthenosphere boundary: Earth and Planetary Science Letters, v. 376, p. 20–28, https://doi.org/10.1016/j.epsl.2013.06.010.

Herzberg, C., and Asimow, P.D., 2015, PRIMELT3 MEGA.XLSM software for primary magma calculation: Peridotite primary magma MgO contents from the liquidus to the solidus: Geochemistry, Geophysics, Geosystems, v. 16, no. 2, p. 563–578, https://doi.org/10.1002/2014GC005631.

Hirose, K., and Kushiro, I., 1993, Partial melting of dry peridotites at high pressures: Determination of compositions of melts segregated from peridotite using aggregates of diamond: Earth and Planetary Science Letters, v. 114, p. 477–489, https://doi.org/10.1016/0012-821X(93)90077-M.

Hofmann, C., Courtillot, V., Feraud, G., Rochette, P., Yirgu, G., Ketefo, E., and Pik, R., 1997, Timing of the Ethiopian flood basalt event and implications for plume birth and global change: Nature, v. 389, p. 838–841, https://doi.org/10.1038/39853.

Isola, I., Mazzarini, F., Bonini, M., and Corti, G., 2014, Spatial variability of volcanic features in early-stage rift settings: The case of the Tanzania Divergence, East African rift system: Terra Nova, v. 26, p. 461–468, https://doi.org/10.1111/ter.12121.

Keir, D., Kendall, J.M., Ebinger, C., and Stuart, G., 2005, Variations in late syn-rift melt alignment inferred from shear-wave splitting in crustal earthquakes beneath the Ethiopian rift: Geophysical Research Letters, v. 32, no. 23, https://doi.org/10.1029/2005GL024150.

Keir, D., Pagli, C., Bastow, I.D., and Ayele, A., 2011, The magma-assisted removal of Arabia in Afar: Evidence from dike injection in the Ethiopian rift captured using InSAR and seismicity: Tectonics, v. 30, no. 2, https://doi.org/10.1029/2010TC002785.

Keir, D., Bastow, I.D., Corti, G., Mazzarini, F., and Rooney, T.O., 2015, The origin of along-rift variations in faulting and magmatism in the Ethiopian Rift: Tectonics, v. 34, p. 464–477, https://doi.org/10.1002/2014TC003698.

Kendall, J., Pilidou, S., Keir, D., Bastow, I.D., Stuart, G.W., and Ayele, A., 2006, Mantle upwellings, melt migration and the rifting of Africa: Insights from seismic anisotropy, *in* Fitton, J.G., and Upton, B.G.J., eds., Alkaline Igneous Rocks: Geological Society of London, Special Publications, v. 259, p. 55, https://doi.org/10.1144/GSL.SP.2006.259.01.06.

Kennan, P., Mitchell, J., and Mohr, P., 1990, The Sagatu ridge dyke swarm, Ethiopian rift margin: Revised age and new Sr-isotopic data [and the Middle East]: Journal of African Earth Sciences, v. 11, p. 39–42, https://doi.org/10.1016/0899-5362(90)90075-P.

Keranen, K., and Klemperer, S.L., 2008, Discontinuous and diachronous evolution of the Main Ethiopian Rift: Implications for development of continental rifts: Earth and Planetary Science Letters, v. 265, p. 96–111, https://doi.org/10.1016/j.epsl.2007.09.038.

Keranen, K., Klemperer, S.L., Gloaguen, R., and Group, E.W., 2004, Three-dimensional seismic imaging of a protoridge axis in the Main Ethiopian rift: Geology, v. 32, p. 949, https://doi.org/10.1130/G20737.1.

Keranen, K.M., Klemperer, S.L., Julia, J., Lawrence, J.F., and Nyblade, A.A., 2009, Low lower crustal velocity across Ethiopia: Is the Main Ethiopian Rift a narrow rift in a hot craton?: Geochemistry, Geophysics, Geosystems, v. 10, no. 5, https://doi.org/10.1029/2008GC002293.

Kieffer, B., 2004, Flood and Shield Basalts from Ethiopia: Magmas from the African Superswell: Journal of Petrology, v. 45, p. 793–834, https://doi.org/10.1093/petrology/egg112.

Kim, S., Nyblade, A.A., Rhie, J., Baag, C.-E., and Kang, T.-S., 2012, Crustal S-wave velocity structure of the Main Ethiopian Rift from ambient noise tomography: Geophysical Journal International, v. 191, p. 865–878, https://doi.org/10.1111/j.1365-246X.2012.05664.x.

Korme, T., Chorowicz, J., Collet, B., and Bonavia, F.F., 1997, Volcanic vents rooted on extension fractures and their geodynamic implications in the Ethiopian Rift: Journal of Volcanology and Geothermal Research, v. 79, p. 205–222, https://doi.org/10.1016/S0377-0273(97)00034-6.

Kurz, T., Gloaguen, R., Ebinger, C., Casey, M., and Abebe, B., 2007, Deformation distribution and type in the Main Ethiopian Rift (MER): A remote sensing study: Journal of African Earth Sciences, v. 48, p. 100–114, https://doi.org/10.1016/j.jafrearsci.2006.10.008.

Kushiro, I., 1996, Partial melting of a fertile mantle peridotite at high pressures: An experimental study using aggregates of diamond, *in* Basu, A., and Hart, S., eds., Earth Processes: Reading the Isotopic Code, 1: Geophysical Monograph Series, p. 197–212, https://doi.org/10.1029/GM095p0109.

Langmuir, C.H., and Forsyth, D.W., 2007, Mantle melting beneath mid-ocean ridges: Washington, D.C., Oceanography, v. 20, p. 78–89, https://doi.org/10.5670/oceanog.2007.82.

Le Corvec, N., Menand, T., and Lindsay, J., 2013, Interaction of ascending magma with pre-existing crustal fractures in monogenetic basaltic volcanism: an experimental approach: Journal of Geophysical Research. Solid Earth, v. 118, p. 968–984, https://doi.org/10.1002/jgrb.50142.

Le Maitre, R.W., Streckeisen, A., Zanettin, B., Le Bas, M.J., Bonin, B., and Bateman, P., eds., 2002, Igneous Rocks: A Classification and Glossary of Terms: Recommendations of the International Union of Geological Sciences Subcommission on the Systematics of Igneous Rocks: Cambridge University Press, https://doi.org/10.1017/CBO9780511535581.

Maccaferri, F., Rivalta, E., Keir, D., and Acocella, V., 2014, Off-rift volcanism in rift zones determined by crustal unloading: Nature Geoscience, v. 7, p. 297–300, https://doi.org/10.1038/ngeo2110.

Mahatsente, R., Jentzsch, G., and Jahr, T., 1999, Crustal structure of the Main Ethiopian Rift from gravity data: 3-dimensional modeling: Tectonophysics, v. 313, no. 4, p. 363–382, https://doi.org/10.1016/S0040-1951(99)00213-9.

Mazzarini, F., Rooney, T.O., and Isola, I., 2013, The intimate relationship between strain and magmatism: A numerical treatment of clustered monogenetic fields in the Main Ethiopian Rift: Tectonics, v. 32, p. 49–64, https://doi.org/10.1029/2012TC003146.

Mazzarini, F., Le Corvec, N., Isola, I., and Favalli, M., 2016, Volcanic field elongation, vent distribution, and tectonic evolution of a continental rift: The Main Ethiopian Rift example: Geosphere, v. 12, p. 706–720, https://doi.org/10.1130/GES01193.1.

McKenzie, D., and Bickle, M., 1988, The volume and composition of melt generated by extension of the lithosphere: Journal of Petrology, v. 29, p. 625–679, https://doi.org/10.1093/petrology/29.3.625.

Medynski, S., Pik, R., Burnard, P., Vye-Brown, C., France, L., Schimmelpfennig, I., Whaler, K., Johnson, N., Benedetti, L., and Ayelew, D., 2015, Stability of rift axis magma reservoirs: Spatial and temporal evolution of magma supply in the Dabbahu rift segment (Afar, Ethiopia) over the past 30 kyr: Earth and Planetary Science Letters, v. 409, p. 278–289, https://doi.org/10.1016/j.epsl.2014.11.002.

Menand, T., 2011, Physical controls and depth of emplacement of igneous bodies: A review: Tectonophysics, v. 500, p. 11–19, https://doi.org/10.1016/j.tecto.2009.10.016.

Meshesha, D., and Shinjo, R., 2007, Crustal contamination and diversity of magma sources in the northwestern Ethiopian volcanic province: Journal of Mineralogical and Petrological Sciences, v. 102, p. 272–290, https://doi.org/10.2465/jmps.061129.

Mohr, P., 1980, Geochemical aspects of the Sagatu ridge dike swarm, Ethiopian rift margin, *in* Geodynamic Evolution of the Afro-Arabian Rift System: L'Accademia Nazionale dei Lincei, v. 47, p. 384–406.

Mohr, P., Mitchell, J., and Raynolds, R., 1980, Quaternary volcanism and faulting at O'a Caldera, Central Ethiopian Rift: Bulletin Volcanologique, v. 43, p. 173, https://doi.org/10.1007/BF02597619.

Mohr, P.A., 1962, Surface cauldron subsidence with associated faulting and fissure basalt eruptions at Gariboldi Pass, Shoa, Ethiopia: Bulletin Volcanologique, v. 24, p. 421–428, https://doi.org/10.1007/BF02599358.

Mohr, P.A., 1967, Major volcano-tectonic lineament in the Ethiopian rift system: Nature, v. 213, p. 664–665, https://doi.org/10.1038/213664a0.

Mohr, P.A., and Potter, E.C., 1976, The Sagatu Ridge dike swarm, Ethiopian rift margin: Journal of Volcanology and Geothermal Research, v. 1, p. 55–71, https://doi.org/10.1016/0377-0273(76)90018-4.

Molin, P., and Corti, G., 2015, Topography, river network and recent fault activity at the margins of the Central Main Ethiopian Rift (East Africa): Tectonophysics, v. 664, p. 67–82, https://doi.org/10.1016/j.tecto.2015.08.045.

Morton, W.H., Rex, D.C., Mitchell, J.G., and Mohr, P., 1979, Riftward younging of volcanic units in the Addis Ababa region, Ethiopian rift valley: Nature, v. 280, p. 284–288, https://doi.org/10.1038/280284a0.

Nimis, P., 1995, A clinopyroxene geobarometer for basaltic systems based on crystal-structure modeling: Contributions to Mineralogy and Petrology, v. 121, p. 115–125, https://doi.org/10.1007/s004100050093.

Nimis, P., and Taylor, W.R., 2000, Single clinopyroxene thermobarometry for garnet peridotites: Part I. Calibration and testing of a Cr-in-Cpx barometer and an enstatite-in-Cpx thermometer: Contributions to Mineralogy and Petrology, v. 139, p. 541–554, https://doi.org/10.1007/s004100000156.

O'Hara, M., 1968, The bearing of phase equilibria studies in synthetic and natural systems on the origin and evolution of basic and ultrabasic rocks: Earth-Science Reviews, v. 4, p. 69–133, https://doi.org/10.1016/0012-8252(68)90147-5.

Parsons, T., and Thompson, G.A., 1991, The role of magma overpressure in suppressing earthquakes and topography: Worldwide examples: Science, v. 253, p. 1399–1402, https://doi.org/10.1126/science.253.5026.1399.

Peccerillo, A., Barberio, M.R., Yirgu, G., Ayalew, D., Barbieri, M., and Wu, T.U., 2003, Relationships between Mafic and Peralkaline Silicic Magmatism in Continental Rift Settings: A Petrological, Geochemical and Isotopic Study of the Gedemsa Volcano, Central Ethiopian Rift: Journal of Petrology, v. 44, p. 2003–2032, https://doi.org/10.1093/petrology/egg068.

Peccerillo, A., Donati, C., Santo, A.P., Orlando, A., Yirgu, G., and Ayalew, D., 2007, Petrogenesis of silicic peralkaline rocks in the Ethiopian rift: Geochemical evidence and volcanological implications: Journal of African Earth Sciences, v. 48, p. 161–173, https://doi.org/10.1016/j.jafrearsci.2006.06.010.

Pik, R., Deniel, C., Coulon, C., Yirgu, G., and Marty, B., 1999, Isotopic and trace element signatures of Ethiopian flood basalts: Evidence for plume-lithosphere interactions: Geochimica et Cosmochimica Acta, v. 63, p. 2263–2279, https://doi.org/10.1016/S0016-7037(99)00141-6.

Pizzi, A., Coltorti, M., Abebe, B., Disperati, L., Sacchi, G., and Salvini, R., 2006, The Wonji fault belt (Main Ethiopian Rift): Structural and geomorphological constraints and GPS monitoring, *in* Fitton, J.G., and Upton, B.G.J., eds., Alkaline Igneous Rocks: Geological Society of London, Special Publications, v. 259, p. 191–207, https://doi.org/10.1144/GSL.SP.2006.259.01.16.

Putirka, K.D., 2008, Thermometers and barometers for volcanic systems: Reviews in Mineralogy and Geochemistry, v. 69, p. 61–120, https://doi.org/10.2138/rmg.2008.69.3.

Putirka, K.D., Mikaelian, H., Ryerson, F., and Shaw, H., 2003, New clinopyroxene-liquid thermobarometers for mafic, evolved, and volatile-bearing lava compositions, with applications to lavas from Tibet and the Snake River Plain, Idaho: The American Mineralogist, v. 88, p. 1542–1554, https://doi.org/10.2138/am-2003-1017.

Robertson, E., Biggs, J., Cashman, K., Floyd, M., and Vye-Brown, C., 2016, Influence of regional tectonics and preexisting structures on the formation of elliptical calderas in the Kenyan Rift,

in Wright, T.J., et al., eds., Magmatic Rifting and Active Volcanism: Geological Society of London, Special Publications, v. 420, p. 43–67, https://doi.org/10.1144/SP420.12.
Rochette, P., Tamrat, E., Féraud, G., Pik, R., Courtillot, V., Ketefo, E., Coulon, C., Hoffmann, C., Vandamme, D., and Yirgu, G., 1998, Magnetostratigraphy and timing of the Oligocene Ethiopian traps: Earth and Planetary Science Letters, v. 164, p. 497–510, https://doi.org/10.1016/S0012-821X(98)00241-6.
Rooney, T., Furman, T., Bastow, I., Ayalew, D., and Yirgu, G., 2007, Lithospheric modification during crustal extension in the Main Ethiopian Rift: Journal of Geophysical Research, v. 112, no. B10, https://doi.org/10.1029/2006JB004916.
Rooney, T.O., 2010, Geochemical evidence of lithospheric thinning in the southern Main Ethiopian Rift: Lithos, v. 117, p. 33–48, https://doi.org/10.1016/j.lithos.2010.02.002.
Rooney, T.O., 2017, The Cenozoic magmatism of East-Africa: Part I—Flood basalts and pulsed magmatism: Lithos, v. 286–287, p. 264–301, https://doi.org/10.1016/j.lithos.2017.05.014.
Rooney, T.O., Furman, T., Yirgu, G., and Ayalew, D., 2005, Structure of the Ethiopian lithosphere: Xenolith evidence in the Main Ethiopian Rift: Geochimica et Cosmochimica Acta, v. 69, p. 3889–3910, https://doi.org/10.1016/j.gca.2005.03.043.
Rooney, T.O., Bastow, I.D., and Keir, D., 2011, Insights into extensional processes during magma assisted rifting: Evidence from aligned scoria cones: Journal of Volcanology and Geothermal Research, v. 201, p. 83–96, https://doi.org/10.1016/j.jvolgeores.2010.07.019.
Rooney, T.O., Hart, W.K., Hall, C.M., Ayalew, D., Ghiorso, M.S., Hidalgo, P., and Yirgu, G., 2012, Peralkaline magma evolution and the tephra record in the Ethiopian Rift: Contributions to Mineralogy and Petrology, v. 164, p. 407–426, https://doi.org/10.1007/s00410-012-0744-6.
Rooney, T.O., Bastow, I.D., Keir, D., Mazzarini, F., Movsesian, E., Grosfils, E.B., Zimbelman, J.R., Ramsey, M.S., Ayalew, D., and Yirgu, G., 2014, The protracted development of focused magmatic intrusion during continental rifting: Focused magma intrusion during rifting: Tectonics, v. 33, p. 875–897, https://doi.org/10.1002/2013TC003514.
Rooney, T.O., Lavigne, A., Svoboda, C., Girard, G., Yirgu, G., Ayalew, D., and Kappelman, J., 2016, The making of an underplate: Pyroxenites from the Ethiopian lithosphere: Chemical Geology, v. 455, p. 264–281, https://doi.org/10.1016/j.chemgeo.2016.09.011.
Rubin, A.M., 1990, A comparison of rift-zone tectonics in Iceland and Hawaii: Bulletin of Volcanology, v. 52, p. 302–319, https://doi.org/10.1007/bf00304101.
Rubin, A.M., 1992, Dike-induced faulting and graben subsidence in volcanic rift zones: Journal of Geophysical Research: Solid Earth, v. 97, p. 1839–1858, https://doi.org/10.1029/91JB02170.
Rubin, A.M., and Pollard, D.D., 1988, Dike-induced faulting in rift zones of Iceland and Afar: Geology, v. 16, p. 413–417, https://doi.org/10.1130/0091-7613(1988)016<0413:DIFIRZ>2.3.CO;2.
Stab, M., Bellahsen, N., Pik, R., Quidelleur, X., Ayalew, D., and Leroy, S., 2015, Modes of rifting in magma-rich settings: Tectono-magmatic evolution of Central Afar: Tectonics, v. 35, no. 1, p. 2–38, https://doi.org/10.1002/2015TC003893.
Sueß, E., 1891, Die Brüche des östlichen Afrika: Denkschrift der kaiserlichen Akademie der Wissenschaften, Math.-Natur. Klasse, Wein.
Thompson, R., 1972, Melting behavior of two Snake River lavas at pressures up to 35 kb: Carnegie Institute of Washington Yearbook, v. 71, p. 406–410.
Trestrail, K.R., Rooney, T.O., Girard, G., Svoboda, C., Yirgu, G., Ayalew, D., and Keppelman, J., 2016, Sub-continental lithospheric mantle deformation in the Yerer-Tullu Wellel Volcano-tectonic Lineament: A study of peridotite xenoliths: Chemical Geology, v. 455, p. 249–263, https://doi.org/10.1016/j.chemgeo.2016.10.013.
Trua, T., Deniel, C., and Mazzuoli, R., 1999, Crustal control in the genesis of Plio-Quaternary bimodal magmatism of the Main Ethiopian Rift (MER): Geochemical and isotopic (Sr, Nd, Pb) evidence: Chemical Geology, v. 155, p. 201–231, https://doi.org/10.1016/S0009-2541(98)00174-0.
Walker, D., Shibata, T., and DeLong, S.E., 1979, Abyssal tholeiites from the Oceanographer fracture zone: Contributions to Mineralogy and Petrology, v. 70, p. 111–125, https://doi.org/10.1007/BF00374440.
Wang, K., Plank, T., Walker, J.D., and Smith, E., 2002, A mantle melting profile across the Basin and Range, SW USA: Journal of Geophysical Research. Solid Earth, v. 107, no. B1, p. ECV 5-1-ECV 5-21, https://doi.org/10.1029/2001JB000209.
Wilson, M., 1994, Igneous Petrogenesis: London, New York, Chapman & Hall, 466 p.
Woldegabriel, G., Aronson, J.L., and Walter, R.C., 1990, Geology, geochronology, and rift basin development in the central sector of the Main Ethiopia Rift: Geological Society of America Bulletin, v. 102, p. 439–458, https://doi.org/10.1130/0016-7606(1990)102<0439:GGARBD>2.3.CO;2.
Wolfenden, E., Ebinger, C., Yirgu, G., Deino, A., and Ayalew, D., 2004, Evolution of the northern Main Ethiopian rift: Birth of a triple junction: Earth and Planetary Science Letters, v. 224, p. 213–228, https://doi.org/10.1016/j.epsl.2004.04.022.
Wolfenden, E., Ebinger, C., Yirgu, G., Renne, P.R., and Kelley, S.P., 2005, Evolution of a volcanic rifted margin: Southern Red Sea, Ethiopia: Geological Society of America Bulletin, v. 117, p. 846–864, https://doi.org/10.1130/B25516.1.
Wright, T.J., Sigmundsson, F., Pagli, C., Belachew, M., Hamling, I.J., Brandsdóttir, B., Keir, D., Pedersen, R., Ayele, A., and Ebinger, C., 2012, Geophysical constraints on the dynamics of spreading centres from rifting episodes on land: Nature Geoscience, v. 5, p. 242–250, https://doi.org/10.1038/ngeo1428.